Environmental Chemistry and Ecotoxicology 7 (2025) 762–775

Contents lists available at ScienceDirect

Environmental Chemistry and Ecotoxicology

journal homepage: www.keaipublishing.com/en/journals/environmental-chemistry-and-ecotoxicology/

Antibiotics in water: Bean pods as adsorbent for removing and recovering ciprofloxacin

Jennifer Gubitosa [a,b,*], Domenico Cignolo [b], Vito Rizzi [b], Luca Pace [b], Paola Fini [c], Andrea Petrella [d], Chiara Milanese [e], Sara Paraboschi [e], Pinalysa Cosma [b]

[a] CNR NANOTEC, Istituto di Nanotecnologia, Sede Secondaria di Bari c/o Dipartimento di Chimica, Università degli Studi di Bari "Aldo Moro", 70126 Bari, Italy
[b] Department of Chemistry, University of Bari "Aldo Moro", Via Orabona, 4-, 70126 Bari, Italy
[c] National Research Council CNR-IPCF, UOS, Bari, Via Orabona, 4-, 70126 Bari, Italy
[d] Dipartimento di Ingegneria Civile, Ambientale, Edile, del Territorio e di Chimica, Politecnico di Bari, Via Orabona, 4, 70125 Bari, Italy
[e] Department of Chemistry, University of Pavia, V. le Taramelli 12, 27100 Pavia, Italy

ARTICLE INFO

Keywords:
Bean pods
Contaminants of emerging concern
Ciprofloxacin
Adsorption
Green chemistry
Recycling
Agri-food wastes recovery
Sustainable adsorbent substrates
Water remediation technologies

ABSTRACT

During this work, the Bean Pods are reported as adsorbent to remove Contaminants of Emerging Concern from water. Specifically, the Bean Pods were washed before their use with 1 M NaOH and HCl solutions, for activating their surface and rendering the material porous with a larger surface area, as evidenced by BET and SEM analyses. Indeed, the pods were fully characterized by adopting different techniques, and UV–Vis spectroscopy was adopted to monitor, at several contact times, contaminated water. To pursue this aim, Ciprofloxacin, a largely used antibiotic, was selected as a model contaminant, exhibiting an high absorption in the UV–Vis spectrum. Moreover, the roles of the physical and chemical parameters such as ionic strength, pH, adsorbent/pollutant amounts, and temperature, during the adsorption, were assessed, obtaining interesting information on the whole process, that occurred efficiently with a maximum adsorption capacity of 45 mg/g. The increase of the adsorbent amount (from 3 to 25 mg) and decrease of pollutant concentration (from 30 to 10 mg/L) favored the Ciprofloxacin removal due to the large presence of active sites. The change of pH values (i.e. 3, 6 and 12) and ionic strength values (in the range 0.001–0.5 M by adopting NaCl) largely inhibited the adsorption, evidencing the presence of electrostatic interactions. The adsorption isotherms, thermodynamics and kinetics of the process were also studied. Specifically, the Freundlich and Temkin models well described the process, suggesting the heterogeneous character of the adsorption, with the formation of a pollutant multilayer onto the adsorbent surface; the process occurred spontaneously ($\Delta G < 0$) with an increase of entropy ($\Delta S > 0$), and it was favored by the increase of temperature ($\Delta H > 0$). The pseudo-first-order kinetic equation described the process with the applicability of the Weber-Morris model, denoting the key role of active sites to host the pollutant, and intra-particle diffusion, respectively. The recycling of the proposed adsorbent was successfully demonstrated by means of a salt solution. New horizons in the use of Bean Pods, for water remediation, was thus successfully demonstrated during this work, proposing an environmentally friendly approach for decontaminating water.

1. Introduction

Water contamination represents an important worldwide concern that negatively affects the whole environment, with impressive and dangerous impacts on human health. [1] Heavy metals, inorganic salts, textile dyes, and Contaminants of Emerging Concern (CECs) could usually be retrieved in water, favoring, according to the case, high toxicity. [1,2] In this regard, it is worth mentioning that in the last decades, the presence of CECs in water bodies has increased, and, over time, these pollutants could worsen the problem of water scarcity. [3] Hence, suitable strategies are necessary to remove them from water. To face the problem, many technologies have been developed by scientists around the world, including ionic exchange, membrane separation, coprecipitation, filtration, reverse osmosis, Fenton oxidation, photodegradation, biodegradation, ozonation, and electrochemical reduction, among others. [4] Unfortunately, these strategies are unsatisfactory

* Corresponding author at: University of Bari "Aldo Moro", CNR NANOTEC – Istituto di Nanotecnologia – Sede Secondaria di Bari, Department of Chemistry, Via Orabona, 4, I-70126 Bari, Italy.
E-mail address: jennifer.gubitosa@uniba.it (J. Gubitosa).

https://doi.org/10.1016/j.enceco.2025.04.007
Received 14 February 2025; Received in revised form 8 April 2025; Accepted 11 April 2025
Available online 12 April 2025

when applied to CECs and could suffer from drawbacks, such as associated costs, lack of scalability, the impossibility of recycling both the adsorbent and the adsorbate, and possible formation of hazardous by-products, increasing the whole environmental toxicity. [4,5] On the other hand, as arising from the literature, [5,6] the adsorption processes seemed to be the most promising methods, overcoming some of the aforementioned negative aspects. For example, interesting results were obtained when carbon-based substances were in use, but some of these adsorbents cannot be considered environmentally friendly. Hence, to respect the principles of Green Chemistry and Circular Bioeconomy, the use of natural materials seemed to be preferred. [7,8] In particular, biopolymers, such as chitosan, alginate [9,10], and agrifood wastes, [11,12] have obtained the greatest interest. Among wastes, the use of coconut shell and husk, banana peel, rice husk and straw, sugarcane bagasse, pineapple peel, bean pod, and bean husk, among others, are worth mentioning. [4]

In particular, as clearly stated in the recent review of Ebuka Chizitere Emenike et al., [4] the Bean Pod (BP) and husk hold significant potential due to their capability to work as adsorbents for water remediation. Moreover, it is worth mentioning that the amount of waste associated with the use of common bean (*Phaseolus vulgaris*) is expected to increase in the next years. Specifically, a peak in dry bean production of about 31.5 million tons worldwide was noted in 2017 (FAO, 2021), and it has been reported that about 60 % of the plant mass becomes waste, frequently discarded, and not fully utilized. [13] So, it should be also important to provide solutions for reusing, recycling, and reducing this waste. [13] For istance, as emphasized in the recent literature, [4] among different applications of BP, an investigation that proposes this material as adsorbent to treat contaminated water, enlarging its applicability, is expected. Accordingly, the relatively low number of papers reporting the specific use of BP for water remediation [13–19] denotes a gap present in the literature that should be filled, enabling research activities in this field. Specifically, BP has been used to remove heavy metals, some dyes, fluorescein, nitrate, phosphate, ibuprofen, and naphthalene [13–19], without clear evidences about the kinetics and thermodynamics related to the removal of CECs from water. On the other hand, the use of bean husk has been largely proposed [4]. Regarding the maximum adsorption capacities, the reported values ranged from 0.38 mg/g to 300 mg/g. Moreover, in these works, a pre-treatment of waste is also described: (i) several washing cycles with tap water and (ii) subsequent activation, including acid and/or alkaline treatment, composite formation, and functionalization with polymers, etc. Its use in the form of active carbon was also taken into account. [15] According to the case, the proposed pre-treatment increased the materials' porosity and surface area, introducing new functional groups on the material's surface, and removing lignin and hemicellulose. Furthermore, it is important to highlight that only three works presented in literature [13,17,18] reported the possibility of regenerating these BP-based adsorbents and desorbing the pollutants. For that purpose, HCl or NaCl solutions were used, and the authors attempted several adsorption and desorption cycles to verify the recyclability. Starting from these considerations, this work has the aim to enlarge the BP applicability, demonstrating the ability of this material to act as adsorbent and remove CECs from water, not yet investigated in literature, detailing the mechanism of pollutant adsorption, the role of parameters affecting the process, the thermodynicmis and kinetics; important information useful to scale-up the process. For the purpose, to detail these features, the attention was focused on Ciprofloxacin (CIP), a largely used antibiotic. [20]

Indeed, the presence of antibiotics in water is an extensively diffused problem. [21–24] Among the others, CIP is a third-generation fluorinated quinolone-based compound, retrieved in water at different concentrations. Accordingly, CIP has been largely prescribed for treating patients affected by SARS-CoV-2-associated pneumonia, and its presence in water in the next years is expected. [25] The importance of CIP removal also arises by looking at the very high number of papers [25–46] available in the literature, evidencing the use of different adsorbents, both from natural and synthetic origin. Specifically, adsorption capacities, ranging from a few to some thousands of mg/g, have been reported. [25–37,40,42–46]. Table 1 summarizes the results. So, the CIP removal is still an actual concern, and advances in this field are obtained and expected every year, with only some works up to now that propose the adsorbent regeneration. As a result, to the best of our knowledge, this work represents the first assessment on the use of dry BP aiming at CIP removal, a CEC, proposing a sustainable way to regenerate the adsorbent. Specifically, a pre-treatment of BP with HCl and NaOH was demonstrated to be necessary to improve the adsorbent features, enhancing its performance. The use of NaCl enabled the pollutant's desorption, presenting a sustenaible way for recycling the adsorbent, lowering the associated costs. The physical and chemical characterization of BP by using synergistically SEM, EDX, ATR-FTIR, BET, XRPD, and TG analyses was thus performed, and the role of physical and chemical key parameters that affected the adsorption process was also assessed, elucidating the kinetics and thermodynamics of the process.

2. Materials and methods

2.1. Chemicals

The BP was obtained from a private organic farm in the Lombardy region (Pavia province), Italy. Ciprofloxacin ($C_{17}H_{18}FN_3O_3$, M.W. 331.35 g × mol^{-1}), and all the investigated contaminants, Propranolol (PRO), Diclofenac (DCF), Carbendazim (MBC), Ketoprofen (Kp) and Carbamazepine (CBZ) were purchased from Sigma-Aldrich (Milan, Italy) and used as received without further purification (purity ≥98 %). The Ciprofloxacin stock solution, 30 mg/L, was prepared in deionized water and diluted to obtain solutions in the range of 10–30 mg/L. When necessary, concentrated HCl (purity 37 %, Sigma-Aldrich, Milan, Italy) and NaOH (reagent grade, ≥98 %, pellets, anhydrous, Sigma-Aldrich, Milan, Italy) solutions were used to modify the pH of the investigated samples. The same commercial source was adopted for LiCl (ACS reagent, purity ≥99 %), NaCl, KCl, $MgCl_2$, NaBr having purity ≥99 %, $CaCl_2$ (purity ≥93 %), and $NaClO_4$ (purity ≥98 %) used to assess the role

Table 1
Natural and synthetic adsorbents used for the CIP removal from water.

Adsorbent	Maximum adsorption capacity Q_{max} mg/g	Reference
Tannin foam	91.8	[45]
Dialium guineense Seed Waste	125	[46]
Sugarcane bagasse	13.6	[26]
Adsorbents based on lignin	0.2–0.4	[27]
Titanate nanotubes	153.90	[28]
Sludge pyrochar	10.42	[29]
Sludge biochar (magnetic)	74.2	[30]
Cyclodextrin-based nanosponges	2	[36]
Iron oxide/cellulose magnetic nanocomposite	168.03	[40]
Nanocomposite beads	9.21–10.87	[32]
Graphene oxide adsorbent	1826.64	[43]
MCM-41 functionalized with amino groups	139.25	[33]
Magnetic biosorbents	527.93	[34]
Solid waste based on biochar-montmorillonite	167.36	[42]
Bacteria sludge	7.642	[35]
Grapefruit peels	565	[31]
Magnetic graphene oxide nanocomposite	106.38	[37]
Ethylene diaminetetraacetic acid– β -cyclodextrin	448	[44]
Kiwi Peels	40	[25]
BP	45	This work

of salts during the adsorption process for confirming the mechanism of the reaction. All the measures were performed in triplicate, and the standard deviation was inferred and reported in each graph.

2.2. Adsorbent preparation

The BP were dried under the sun to a constant mass before the chemical treatments. [46] Subsequently, 100 g of BP was reduced in size with a mortar to obtain small pieces of around 1 mm × 1 mm, avoiding the use of powder that cannot be recovered easily from water. The BP were thus placed in 300 mL of hot water and kept under constant stirring for 30 min. This step was repeated 5 times (sample 1, in **Table S1**) and indicated in the paper as BP/H_2O. Subsequently, adopting the same contact time, the obtained material was further treated with 300 mL of 1 M HCl, NaOH, or HCl/NaOH, and finally washed with the same volume of water until a neutral pH value was attained (See **Table S1** for the details about the sample treatments, indicated as samples from 2 to 4). The wet substrates were then dried in the oven at 60 °C until constant weight, and approximately for 24 h, obtaining the dry adsorbent.

2.3. UV–Visible measurements

A CARY 5 UV–Vis-NIR spectrophotometer (Varian Inc., now Agilent Technologies Inc., Santa Clara, CA, USA) was used for collecting the UV–Vis absorption spectra in a range of 200–400 nm, at a 1 nm/s scan rate. The Ciprofloxacin concentration was inferred by measuring the absorbance intensity at λ 335 nm; a molar absorption coefficient (ε) of 14,200 $L \times mol^{-1} \times cm^{-1}$was experimentally calculated by adopting the Lambert-Beer law.

2.4. ATR-FTIR spectroscopy measurements

ATR-FTIR spectra of the inner and outer BP surface, before and after the adsorption/desorption, were recorded in a 4000–500 cm^{-1} range by using a Fourier Transform Infrared spectrometer (FTIR Spectrum Two from Perkin Elmer, Waltham, MA, USA).; the resolution was set at 4 cm^{-1}, and 16 scans were summed for each acquisition.

2.5. Specific surface area analysis

The specific surface area of the different samples was determined by N_2 adsorption (BET method). The nitrogen adsorption curves were acquired by a Sorptomatic 1990 (Thermo Electron Corporation, operating with the static volumetric principle). The correction for the volume of the sample was introduced by measuring the He sorption.

2.6. Scanning Electron Microscopy (SEM) and energy dispersive X-ray spectroscopy (EDX) analyses

SEM measurements were performed using a Zeiss EVO MA10 (Carl Zeiss, Oberkochen, Germany) at an acceleration voltage of 20 kV and 8.5-mm working distance on gold-sputtered samples. EDX analyses were performed with an XMax50 mm^2 detector by Oxford Instruments (UK).

2.7. X-Ray Powder Diffraction Analysis (XRPD)

XRPD analyses were performed with a D2-Phaser diffractometer (Bruker AXS, Karlsruhe, Germany), with Cu-Kα radiation. The analyses were performed in an angular range from 5° to 50° with an angular step of 0.02° and a scan speed of 1.2°•min^{-1}.

2.8. Thermogravimetric (TG) analyses

The investigation of the thermal properties of the samples was performed by using a Perkin Elmer Pyris 1 thermogravimetric instrument. The analyses were performed under an inert atmosphere using nitrogen as a purge gas, with a constant flow rate of 30 mL/min. Each sample (4–5 mg) was heated from 30 °C to 600 °C at a heating rate of 10 °C/min.

2.9. In batch equilibrium experiments in the presence of Ciprofloxacin

Where not indicated, the experiments of adsorption were performed at room temperature (298 K) at an initial pH of 6. In detail, the % of adsorption, % of Ads, was calculated by adopting **Eq. 1**. [28]

$$\%\text{of Ads} = \frac{A_0 - A_t}{A_0} \times 100 \quad (1)$$

where A_0 and A_t are the UV–Vis absorbance intensities of the pollutant solution, measured at λ 335 nm, at time t_0 and t time, respectively.

The adsorption capacities, q_t (mg × g^{-1}), were calculated by using **Eq. 2**. [26,28,45]

$$q_t = \frac{C_0 - C_t}{W} \times V \quad (2)$$

V represents the pollutant solution volume (15 mL), W is the dried adsorbent mass (g), C_0 and C_t (mg/L) are the pollutant amounts at time t_0 and t, respectively.

To assess the role of the pollutant amount during the adsorption, 25 mg of adsorbent was placed into 15 mL of a Ciprofloxacin solution having different initial concentrations (from 30 mg/L to 10 mg/L). The adsorbent amount, from 3 to 25 mg, was also changed by fixing the Ciprofloxacin at 10 mg/L. The process was studied under constant and continuous stirring (120 rpm, using a M4 Digita PRO Multiple Heating Magnetic Stirrer (VELP SCIENTIFICA). With the aim of assessing the role of pH, temperature, and ionic strength during the adsorption, experiments were performed in the presence of 25 mg of adsorbent and 10 mg/L of Ciprofloxacin.

2.10. Adsorption kinetics

The kinetic of the CIP adsorption was studied by applying the pseudo-first-order (PFO) and pseudo-second-order (PSO) kinetics models. So, **Eq. 3** and **Eq. 4** were adopted to describe PFO and PSO models, respectively. [25,31,36]

$$ln(q_e - q_t) = ln(q_e) - K_1 \times t \quad (3)$$

$$\frac{t}{q_t} = \frac{1}{K_2 q_e^2} + \frac{1}{q_e} \times t \quad (4)$$

Where q_e (mg/L) represents the adsorbent adsorption capacity at equilibrium, q_t (mg/L) is the adsorption capacity at time t. k_1 (min^{-1}), and k_2 (g/(mg × min)) are the rate constants of PFO and PSO models, respectively.

The Weber-Morris equation (**Eq. 5**) was also applied to study the role of the intraparticle diffusion.

$$q_t = k_{int} \times t^{1/2} + C \quad (5)$$

with k_{int} representing the kinetic constant expressed in mg/(g × $min^{1/2}$), describing the intra-particle diffusion rate, and C is the thickness of the boundary layer.

2.11. Thermodynamic studies

The adsorption process was performed at different temperatures ranging from 276 to 323 K. 25 mg of adsorbent was placed inside a 10 mg/L pollutant solution and the adsorption process was monitored at each temperature, calculating q_t. Free energy (ΔG°), entropy (ΔS°), and enthalpy (ΔH°) were obtained. [25,26,36] **Eq. 6** was used to calculate the free energy:

$$\Delta G^{\circ} = -RT\, ln\, K_{eq} \quad (6)$$

Where R is the universal gas constant, 8.314 J × mol^{-1} × K^{-1}, *T* is the temperature (K), and K_{eq} is the equilibrium constant expressed as q_e/C_e. The values of ΔH° and ΔS° were inferred by equaling **Eqs. 6** with **7** to obtain **Eq. 8**.

$$\Delta G^\circ = \Delta H^\circ - T\Delta S^\circ \quad (7)$$

$$ln K_{eq} = -\frac{\Delta H^0}{RT} + \frac{\Delta S^0}{R} \quad (8)$$

2.12. Adsorption Isotherms. Langmuir, Freundlich, Temkin, and Dubinin–Radushkevich models were applied to experimental data referring to experiments of adsorption obtained when the amount of pollutant was changed. [25,36] The q_t at equilibrium, called q_e, and the corresponding pollutant amount left in the solution, C_e, were arranged according to **Eqs. 9–13**. The purpose was to find the best model that well described the process, which should occur with particular features, according to a specific isotherm model. The Langmuir (**Eq. 9**) model suggests that (i) all the adsorption sites are characterized by constant energy, and (ii) the pollutant is adsorbed on the surface of the adsorbent, without interactions between the molecules of pollutant, forming a monolayer.

$$\frac{C_e}{q_e} = \frac{1}{K_L Q_0} + \frac{C_e}{Q_0} \quad (9)$$

Herein, q_e (mg/g) is the pollutant adsorbed amount at equilibrium, C_e is the correspondent equilibrium concentration of Ciprofloxacin in solution, expressed in mg/L, K_L is the Langmuir equilibrium constant (L/mg), and Q_0 is the theoretical maximum adsorption capacity (mg/g) of adsorbent.

The Freundlich isotherm (**Eq. 10**) illustrates an adsorption process that occurs on a heterogeneous surface where available sites to host the pollutants have not equal heat of adsorption; in this case, the latter changes exponentially with the pollutant adsorption.

$$log(q_e) = log(K_F) + \frac{1}{n} log(C_e) \quad (10)$$

K_F (L/mg) is the Freundlich constant, and n is the heterogeneity factor. Usually, the 1/n value measures if the adsorption process is irreversible ($1/n = 0$), favorable ($0 < 1/n < 1$), or unfavorable ($1/n > 1$).

On the other hand, the Temkin model (**Eq. 11**) indicates that during the adsorption process, the heat of adsorption decreases linearly due to adsorbent/adsorbate interactions.

$$q_e = B_1 ln(K_T) + B_1 ln(C_e) \quad (11)$$

with K_T (L/mol) representing the equilibrium binding constant, and B_1 referring to the heat of adsorption.

Dubinin–Radushkevich isotherm (D-R) (**Eq. 12**) supposes that the adsorption of the pollutant onto a heterogeneous surface and the energy distribution can be described by using a Gaussian curve.

$$\ln q_e = ln(Q_0) - K_{D-R} \times \varepsilon^2 \quad (12)$$

Where q_e (mg/g) is the equilibrium adsorption capacity, Q_0 (mg/g) is the theoretical maximum adsorption capacity, and $K_{D\text{-}R}$ (mol^2/J^2) is the Dubinin–Radushkevich isotherm constant. ε is the potential of Polanyi (**Eq. 13**).

$$\varepsilon = RT\ln\left(1 + \frac{1}{C_e}\right) \quad (13)$$

R is the gas constant (8.314 J/mol K), T is the absolute temperature (K), and C_e represents the pollutant equilibrium concentration (mg/L).

The model also predicts the value of energy, E, involved during the adsorption process (**Eq. 14**).

$$E = \frac{1}{\sqrt{2K_{D-R}}} \quad (14)$$

Specifically, a value of E in the range of 8–16 kJ/mol suggests that chemisorption could be taken into account during the process, while for E < 8 kJ/mol, the physisorption could be considered.

2.12. *In batch desorption experiments*

Desorption experiments were performed by placing the adsorbent, after removing the pollutant from water, into a solution (15 mL) containing NaCl 0.1 M, under constant stirring (120 rpm, using a M4 Digita PRO Multiple Heating Magnetic Stirrer (VELP SCIENTIFICA). UV–Vis absorption spectroscopy was used to monitor the amount of desorbed Ciprofloxacin.

2.13. *Bean Pods' point of zero charge determination*

The pH of Bean Pods' point of zero charge (pH_{PZC}) was calculated by using the drift method. For this purpose, 30 mL of NaCl solutions 5.0 × 10^{-2} M were prepared by changing the pH values from 2 to 11 (pH_i) after adding HCl or NaOH. Then, the solution's pH (pH_F) was measured after contact with 25 mg of Bean Pods for 48 h under continuous stirring. The pH_{PZC} value was obtained by plotting pH_i versus pH_i and pH_i versus pH_F; the crossover of these curves represents the pH_{PZC} value.

3. Results and discussion

3.1. *Physicochemical features of BP*

The physical and chemical features of BP after the adopted treatments were evaluated using synergically SEM, EDX, XRPD, BET, ATR-FTIR, and TG techniques. In the case of ATR-FTIR analysis, the attention was focused both on the inner and outer sides of the pods' surface. In particular, the inner face is referred to as the surface in strict contact with the bean, conversely, the outer one is referred to as the external side.

3.1.1. *SEM, EDX and BET analyses*

Figs. 1A-D report the SEM images for the BP after washing with water, which occurred, as a whole, similarly to raw material: a fibrous and flaky structure can be observed (**Figs. 1A** and **B**), with several different sheets resting on each other (Fig. 2C). Some visible breaks in the fibers were evident, forming some small cavities (**Figs. 1A** and **B**). The surface of the different sheets appeared wrinkled and crossed by channels with different widths (Fig. 1C), with the smallest ones forming a sort of net. The elemental analysis (Fig. 1D) showed that the pods were composed of O (more than 55 wt%) and C (about 38 wt%), with a small amount of K (around 3 %) and traces of other elements like Mg and P naturally present in the biomass. Regarding the alkali treatment, it has been reported that it could affect the materials' porosity and surface area due to the induced rearrangement of the main components of BP. [4] The macroscopic morphology was maintained, with large grains having irregular shapes made of enrolled sheets (Fig. 1E, in the middle). Moreover, grains with prismatic shapes appeared (Fig. 1E, on the right) with evident pores, up to 5 μm, on the surfaces (Fig. 1F). The channels on the sheets were still present (Fig. 1G), and their surface was more wrinkled with respect to the water-washed pods and covered with the net of the smaller channels. The EDX analysis (**Fig. H**) showed an increase in the C content up to 68 wt%, O content of around 30 wt%, the presence of a small amount of Na (around 1.5 wt%) from the washing solution, and very small quantities of Mg, Si, and Ca from the original matrix. According to these results, the specific surface area of the dry bean pods after washing with water, as determined by the BET method, was 49 ± 3 m^2/g, with pore volumes of 0.12 ± 0.02 cm^3/g; while the NaOH washing leads to an area of 72 ± 3 m^2/g and a pore volume of 0.14 ± 0.02 cm^3/g values, respectively. In excellent agreement with these results, when the adsorption study was performed, the CIP removal was improved, if compared with the results referred to BP whashed with water only (see **Fig. S3B** and the related discussion

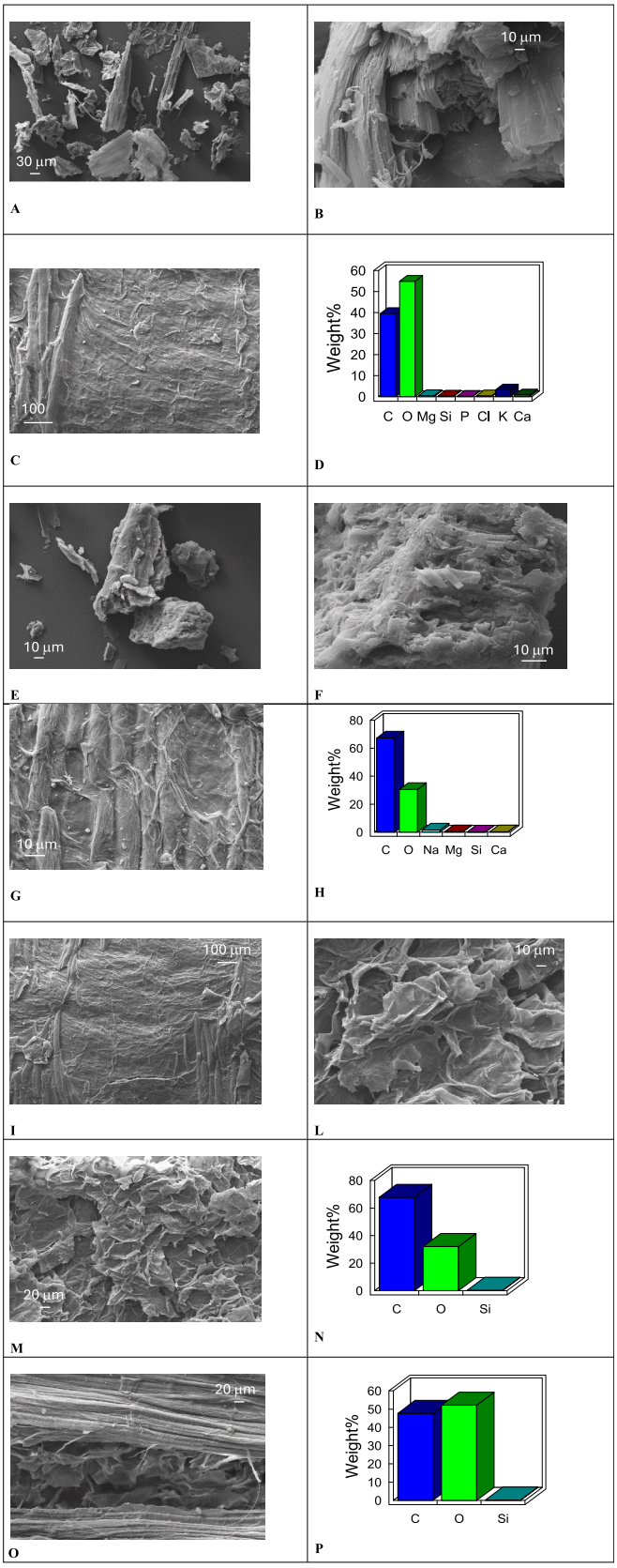

Fig. 1. SEM and EDX images for BP/H_2O (**A-D**), BP/NaOH (***E*-H**), BP/HCl (**I—N**), and BP/NaOH/HCl (**O, P**).

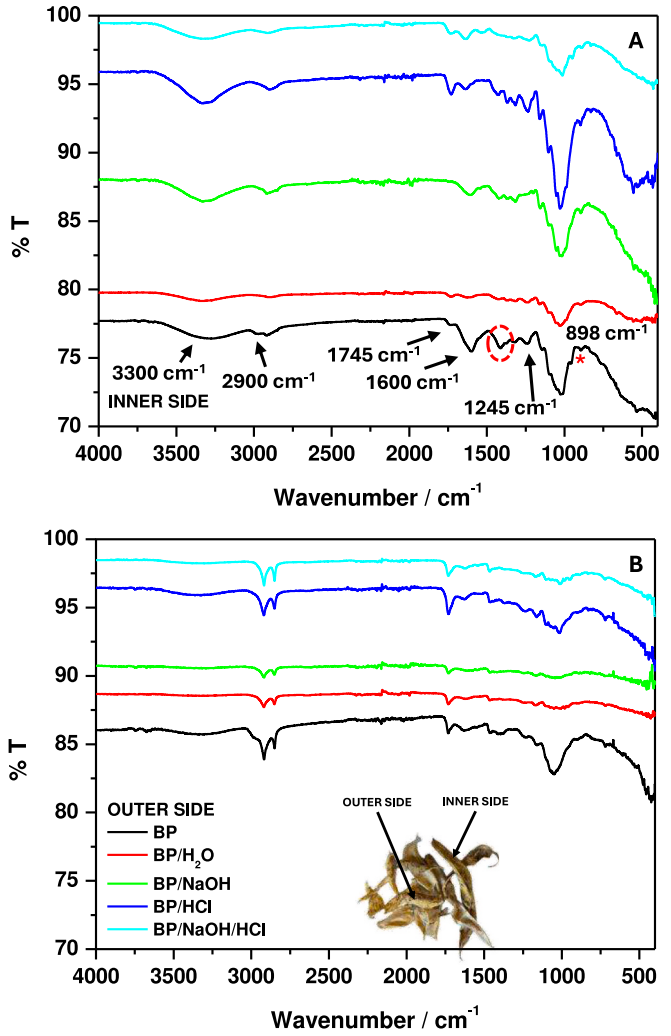

Fig. 2. Comparison of ATR-FTIR spectra of BP referred to the inner (**A**) and outer side (**B**), evaluating the effect of the used pre-treatments.

reported in the *paragraph 3.2* for more details).

The treatment with HCl, as well known in the literature, [4] noticeably increased the number of cavities, making the material more porous. Indeed, the pre-treatment with acids could remove impurities, increase the surface area, and introduce new functional groups on the material's surface. [4] Some of the largest fibers appeared broken, and some cracks were observed on the surface (Fig. 1I). Moreover, some grains with exfoliated surfaces were evident, with a noticeable increase in the porosity (**Fig. 1L** and **M**). The EDX analysis (Fig. 1N) revealed that the composition in C and O was similar to the sample washed with NaOH, and only a very small amount of Si (maximum 0.2 wt%) was still detectable. Accordingly, the specific surface area of the bean pods after washing with HCl leads to a specific surface area of 83 ± 3 m^2/g and pore volumes of 0.15 ± 0.02 cm^3/g values, respectively. Not surprisingly, the CIP removal was further improved (see **Fig. S3B** and the related discussion reported in the paragraph 3.2 for more details).

When the combined basic and acidic treatment was considered, their synergistic effect was observed, and the specific surface area was further increased to 89 ± 3 m^2/g, and the pore volumes occurred 0.15 ± 1 cm^3/g. The samples (Fig. 1O) presented a morphology intermediate between the ones treated with one of the two activating agents, with still integer fibers intercalating very rough and porous structures. In this case, the amount of C and O was similar (48 wt% and 52 wt% respectively), with traces of Si (Fig. 1P), and the removal of CIP occurred more performant (see **Fig. S3B** and the related discussion reported in the paragraph 3.2

for more details).

3.1.2. XRPD analyses

To further unveil the effect of the adopted pre-treatment, the XRPD analysis was performed. The patterns of the BP as well as BP after water washing (**Fig. S1**) showed two main large peaks centered at 16° (less intense) and 22° (more intense), and a small one at 35°, due to the presence of the monoclinic cellulose Iβ molecules: [47] in particular, due to the presence of a huge amorphous fraction, the first band was attributed to the superimposition of the (101) and (10−1) reflections, [48] and the other two to the (002) and (0 4 0) crystallographic plane reflections. [49] Pure lignin also showed a huge amorphous band centered at around 21° due to the (200) reflection: [50] the presence of this polymer was evident in the shoulder at low angle of the 22° signal of cellulose. Similar patterns were obtained for the samples treated with NaOH, and the mixture of NaOH and HCl (**Fig. S1**): the small but evident shifts at lower angles for the two main peaks can be attributed to larger interlayer spacing, compared with untreated biomass, [51] while the enlargement of the first signal was due to an increased grade of amorphicity. Moreover, in the sample washed with HCl (**Fig. S1**), another variation was well evident, and the two bands occurred with different intensities, testifying to a stronger effect of the acidic treatment on the biomass. In this sample and in the one treated with the combination of NaOH and HCl, the band at 21° appeared narrow and the shoulder at a lower angle was less pronounced with respect to raw or BP washed with water: it could be hypothesized that the lignin polymer was attacked by the acidic solution and decreased in amount, leading to the results observed during the morphological investigation and the BET analysis. [4]

3.1.3. TG analyses

More detailed information was obtained by using the TG analyses. **Figs. S2A** and **B** show the BP's thermogravimetric curves and the corresponding derivative signal (DTG) related to the adsorbent's different pre-treatments. For all the samples, a slight mass loss was observed until the temperature of 100 °C, which could be ascribed to the release of adsorbed water present in the lignocellulosic material, and the decomposition of very light volatile compounds. [52] Subsequently, other typical decomposition stages were detected and better appreciated in terms of DTG. Specifically, the major weight losses were observed in the temperature range between 200 and 400 °C and 450–600 °C, which can be attributed to hemicellulose and cellulose degradation and lignin decomposition. [53,54] The hemicellulose degradation occurred between 200 and 350 °C, while the cellulose degradation started above 320 °C. Regarding lignin, the decomposition began at the temperature of hemicellulose degradation and continued up to 550 °C. After the pre-treatment with water (BP/H_2O), the main BP weight losses were well-defined but shifted towards higher temperatures if compared with the thermogram of the as-received raw BP. The higher thermal stability of the main components of BP can be due to a probable rearrangement of the lignocellulosic material through the formation of novel H-bonds. Interestingly, in the thermograms of samples referred to BP pre-treated with NaOH and/or HCl, the signal around 450 °C, mainly attributed to lignin, disappeared. With regards to the contribution of cellulose and hemicellulose, the related signals were affected, occurring with slight changes in the corresponding temperatures. In agreement with the previous discussion, the use of HCl should favor the cleavage of the aryl ether lignin bonds, leading to lower-weight lignin by-products that usually display higher thermal instability. [13,55] So, their contributions slightly increased at 550 °C. As a result, the thermogram related to BP pre-treated with HCl and NaOH can be easily rationalized by considering the synergistic effect of the basic and acidic treatment, that favored a new assembly of the lignocellulose biomass in a more porous network.

3.1.4. ATR-FTIR spectroscopy measurements

In this case, appreciable differences were detected when referring to the inner and outer sides of the material before and after the adopted treatments. The ATR-FTIR measurements of as-received and washed BP revealed (Fig. 2) characteristics signals attributable to the presence of hemicellulose, cellulose, and lignin, the main expected components of BP, according to previous results and as already observed in similar works. [53,56–59]

Starting from the spectrum arising from the inner side of as-received BP (Fig. 2A), a wide and defined band in the region 3500–3000 cm^{-1} attributed to the stretching vibration of the O—H groups from phenols, carboxylic acids or alcohols, and water from hemicellulose, cellulose, and lignin, was observed (with the contribute of intra and intermolecular hydrogen bonds). Not well-resolved signals were detected around 2890 cm^{-1} and 2900 cm^{-1}, which could be ascribed to the symmetric and/or asymmetric C—H stretching, typical vibrations of -CH_3 and -CH_2- groups of cellulose and hemicellulose. A small peak, owing to C═O from lignin and mainly hemicellulose, was observed at 1745 cm^{-1}. [56] Indeed, Kostryukov et al. [56] used the latter signal to infer quantitative information about the presence of hemicellulose. Accordingly, Jiang et al. assigned this band and the vibration occurring at 1245 cm-1 to hemicellulose. [57] The vibration at 1600 cm^{-1} can be attributed to aromatics, and thus to C═C double bonds of lignin, whose presence was further confirmed by the contributions at 1462, 1427 (in the red dotted circle), 1115, and 1030 cm^{-1}. [57] In the region 1425–1200 cm^{-1}, various vibration modes were observed, further proving the presence of cellulose, hemicellulose, and lignin. [53,56,58,59] The main cellulose contribution could be attributed to vibrations at 1374, 1328, 1163, 1056, and 898 cm^{-1}. In particular, the latter, indicated with asterisks, suggested the presence of crystalline structures of cellulose. [57] The shoulder at 1630 cm^{-1} arose from the contribution of water and hydrogen bonds between hemicellulose and lignin. It is worth mentioning that in the region 1200–1100 cm^{-1}, besides the typical signals ascribed to C—O and C-O-C stretching of sugar-based compounds, herein cellulose and hemicellulose, the vibrations of ethers and esters from the lignin structure could also be taken into account (1100–900 cm^{-1}). [53,55–59] When the BP outer side was considered in Fig. 2B, the aforementioned signals were retrieved. Particularly, the doublet around 2900 cm^{-1} was strongly evident, and, in this case, two signals were well identified at 2919 cm^{-1} and 1850 cm^{-1}, respectively. The C—H stretching of cellulose, hemicellulose, and lignin occurs at these wavenumbers. [53,56–59] On the other hand, the shoulder at higher wavenumber can be mainly attributed to cellulose and hemicellulose, as previously observed for the inner side. Clear signals from the C═O around 1745 cm^{-1} and 1245 cm^{-1} were detected, confirming the hemicellulose presence. Interestingly, when the material was washed with water, all the signals referred to both sides of BP appeared the same but reduced in intensity, as the vibrations were blocked into a more compact assembly. In particular, the vibrations at 1600 cm^{-1} and 1425 cm^{-1} appeared weak in terms of relative intensity, if compared with the others. At the same time, the vibrations at 1745 cm^{-1} and 1245 cm^{-1}, attributed to hemicellulose, were more intense. The OH contribution at 3500–3000 cm^{-1} was slightly present and, at the same time, shifted at a higher wavenumber. On this ground, the process favored the disruption of H-bonds and the formation of new ones in between the main components, affecting the arrangement of the whole network. [53,56–59] On the other hand, noteworthy results were observed when the effect of HCl and NaOH was investigated. Significant differences in the band relative intensities and shifts in the wavelength positions were detected on both sides of BP (**Fig. 2A** and **B**). According to XRPD and TG analysis, it is also possible to suppose the break of the lignin structure in favor of other by-products that have carboxyl groups derived from the breaking of aryl ether bonds. This was evidenced by the increased C═O stretching vibration at 1745 cm^{-1} [55] This effect was more pronounced when the outer side of BP was studied. Specifically, the ratio between the band intensity at 1745 cm^{-1} and 1600 cm^{-1}

changed in favor of the former. However, at the same time, the signal at 1245 cm^{-1} increased, also denoting the important contribution of hemicellulose at 1745 cm^{-1}. So, the lignin decomposition should favor the new arrangement of the material. Accordingly, the shoulder at 1630 cm^{-1} was less evident, suggesting the breaking of H-bonds between lignin and hemicellulose. The signals in the region 1050–1115 cm^{-1} were also affected due to the disruption of the interactions of hemicellulose with lignin and cellulose. Regarding the alkali pre-treatment, when the attention was focused on the inner side, the contribution of lignin and hemicellulose signals around 1745 cm^{-1} appeared significantly reduced among the others. Accordingly, the band at 1245 cm^{-1} disappeared, suggesting the partial decomposition/removal of hemicellulose and lignin, whose presence was still detectable at 1600 cm^{-1}. So, changes in the interaction between cellulose and lignin occurred, and the bands at 1600 cm^{-1} and 1163 cm^{-1} were shifted. The outer surface seemed less affected by the pre-treatment, leading to a minor extent of the previously observed changes. In this case, the vibration in the region 3500–3000 cm^{-1} was less evident, denoting the novel assemblies of the main components in terms of the H-bonds network. On this ground, the synergistic action of HCl and NaOH can be better understood. The pre-treatment should favor the partial lignin removal and/or its decomposition in small molecules. At the same time, partial hemicellulose removal/decomposition was favored in excellent agreement with the retrieved surface area and porosity.

3.2. The case of study: Ciprofloxacin removal by bean pods

To quickly monitor the CIP removal from water, UV-VIS spectroscopy was used. Indeed, CIP water-based solutions exhibit typical signals in the UV–Vis region of the spectrum ascribed to $\pi \rightarrow \pi^*$ transitions ($\lambda =$ 270, 323, and 335 nm). [25] To highlight the performance of BP in removing CIP from water, **Fig. S3A** shows the UV–Vis spectrum evolution of a 10.0 mg/L CIP solution in the presence of 25 mg of BP pre-treated with NaOH/HCl that, as argued in the following, was selected among the others. After 1 h of contact time, the absorbance band intensities decreased, and 60 % of CIP was successfully removed. At the same time, a change in the initial pH value, from 6 to 4.5, was rapidly observed after the contact of the adsorbent with the water solution containing the pollutant. The same phenomenon was not observed in the absence of CIP. To better highlight the mechanism of adsorption, and thus the importance of NaOH and HCl solutions for pre-treating BP, needed to activate its surface, a comparison of the CIP % of adsorption on BP, when preliminary treated with (i) water, (ii) NaOH, (iii) HCl only, and (iv) NaOH/HCl, was reported in **Fig. S3B**. The CIP removal increased passing from condition (i) to (iv), indicating how the pre-treatment selected for BP was necessary. Indeed, the synergistic use of NaOH and HCl increased BP's porosity and surface area, as previously demonstrated, favoring the adsorption to the greatest extent. At the same time, the change in the initial pH value of the solution was significantly observed only after the NaOH/HCl pre-treatment of the adsorbent. This well agreed with the BP features found during the corresponding ATR-FTIR analysis, where the presence of carboxylic moieties was extensively retrieved on the material surface. These O-based moieties, considered protonable sites characterized by a low proton affinity (in comparison with phenolic and alcoholic functional groups), [60] can be more easily protonated after the activation with NaOH/HCl, thus favoring the exchange with CIP. Accordingly, the pH value decreasing was observed only under this condition of work and when the material was pre-treated with the lone HCl, but in this latter case, the reduced % of adsorption can be associated with the reduced surface area and pore volume. So, to better detail this finding, the role of initial pH during the adsorption, and the possibility of removing other pollutants from water having the same molecular features in common with CIP, were assessed.

At first, the pH effect was studied because, as reported in the literature, [25–29,36,40,45,46] the solution pH could have a key role during the adsorption processes, affecting the degree of pollutants' protonation and the adsorbent's surface charge. Specifically, Fig. 3 reports the obtained results, showing the % of CIP adsorption (using **Eq. 1**) on the selected BP, pre-treated with NaOH/HCl, at different pH values. The adsorption process occurred largely affected by the pH, appearing hindered at pH 3 and 12.

CIP presents two pK_a values, $pK_{a1} \approx 6$ and $pK_{a2} \approx 8$, associated with the carboxylic and piperazine groups deprotonation, respectively. [25–30,36,40,45,46] So, CIP can be considered a cation (CIP^+) at pH < pK_{a1}, zwitterion ($CIP^{\pm}$) in the range of pH between $pK_{a1} <$ pH < pK_{a2}, or anion (CIP^-) at pH > pK_{a2}. At the same time, the adsorbent changed its surface electrostatic properties. In particular, as reported in **Fig. S4**, the drift method was applied to calculate the PZC of BP [25,36] that occurred around pH 3. So, the BP was positively and negatively charged at pH < 3 and > 3, respectively, due to the presence of carboxylic groups on the adsorbent surface. On this ground, the different adsorption behavior could be rationalized. In the range of pH between 3 and 6, the adsorbent was negatively charged, and an electrostatic attraction between $CIP^{\pm}$ and BP occurred. So, the involvement of the protonated piperazine ring and the negatively charged BP could be supposed. [25–30,36,40,46,61] According to the obtained results, an exchange between H^+ and $CIP^{\pm}$ on the pods' surface occurred, decreasing the pH of the water-based solution, and favoring the removal of the pollutant. At pH < 3, both CIP and BP were positively charged, and the repulsion was mainly observed. Accordingly, the change in the initial pH value was not observed. To the same extent, at pH > 6, CIP was an anion, and it was repelled by negative charges on the BP surface. Starting from these considerations, a comparison with other pollutants was performed to corroborate the pH's role in the mechanism of adsorbate/adsorbent interaction, mainly ruled by electrostatic interactions. Particularly, Propranolol (PRO), Diclofenac (DCF), Carbendazim (MBC), Ketoprofen (Kp), and Carbamazepine (CBZ) were used for the purpose. The choice of these pollutants can be understood by focusing on their chemical structures. PRO, MBC, and DFC were selected for the presence of similar protonable -NH moiety (see orange circles in Fig. 3). Conversely, CBZ and Kp lack of this molecular characteristic. Fig. 3 shows the obtained results, reporting the % of adsorption for each pollutant at neutral pH 6, pH 3, and pH 12. At pH 6, although with percentages much lower than the CIP % of adsorption, the pollutants PRO, DCF, and MBC were successfully removed by BP. At the same time, the previous change of initial pH was again observed, confirming the proton exchange-based mechanism of adsorption. It is worth mentioning that the same experiments

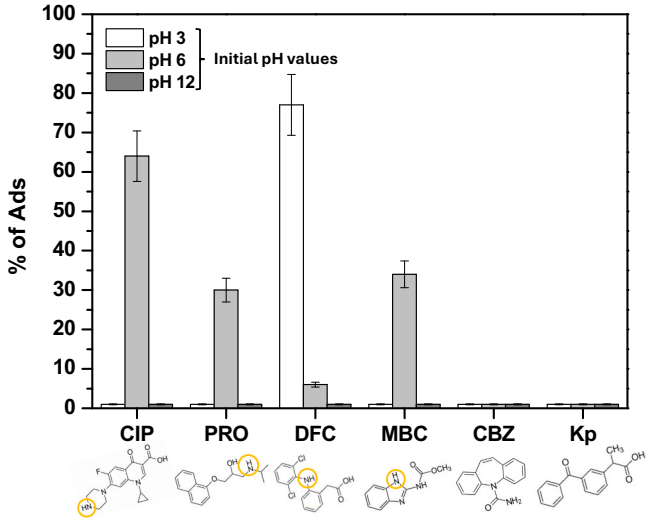

Fig. 3. Comparison of the % of Ads of BP/NaOH/HCl (25 mg) relative to different pollutants (at an initial concentration of 10 mg/L) under different pH conditions at room temperature.

were performed in the presence of only water-washed BP (BP/H_2O), and the removal of these pollutants was not significantly observed, confirming the same behavior of CIP that was adsorbed at a minor extent by this adsorbent (BP/H_2O). Regarding the behavior at the other pH values, as previously observed for CIP, at pH 3 and 12, the process was stopped for almost all the tested pollutants, confirming the important role of the protonable amino groups. The only exception to this trend was represented by DCF, which was highly adsorbed at pH 3 without any modification of the initial pH.

Regarding PRO and MBC, the findings can be rationalized confirming that the main driving force for adsorption on BP was electrostatic. Indeed, PRO has a $pK_{a1} = 9.5$ [62] attributed to the deprotonation of the amino group, while MBC has two pK_a values: $pK_{a1} = 4.53$ (related to its basic guanidinium group) and $pKa_2 = 9.6$ (related to its carbamide group). [63] So, it occurred in its positive form at pH < pKa_1, and as an anion at pH > pKa_2, while it was neutral when pKa_1 < pH < pKa_2. On this basis, at pH 6, which changed rapidly to 4.5 value at the pollutant addition, PRO was mainly present in the cationic form (PRO^+); on the other hand, MBC existed as a neutral form. However, the retrieved pH value was exactly at pH = pKa_1, suggesting that the protonated form was present, although in equilibrium with the neutral MBC. This consideration could also justify the reduced affinity of this pollutant for PB with respect to CIP. On the other hand, at pH 3 and 12, both molecules assumed the same charge of the adsorbent surface; therefore, the repulsion was mainly observed. The different behavior shown by DCF could be attributable to its reduced solubility at acidic pH. [64] Generally, DCF is characterized by a pK_a of 4.22, mainly existing in the molecular neutral form at pH < 4.22, while the negative ionic form predominates at pH > 4.22. [65] Hence, the adsorption was hindered at neutral and alkaline pH values due to the increasing electrostatic repulsion between negative DCF and negative adsorbent. Interestingly, at pH 3 DCF was in its neutral form, but under this condition a very low solubility was accounted for, in the literature. [66] The high removal of DCF, under this condition of work, could be thus rationalized by taking into account its precipitation on the BP surface. [67]

The behavior of CBZ and Kp further assessed that the BP adsorption process occurred almost exclusively through electrostatic interactions. Accordingly, Kp and CBZ were never adsorbed (Fig. 3). CBZ has two dissociation equilibriums characterized by two pK_a values: $pK_{a1} = 2.3$ and $pK_{a2} = 13.9$. [68] It is also considered a moderately hydrophobic compound, being present in non-ionized form at normal pH levels in wastewater. [68] So, since CBZ was not adsorbed also when the pH of the solution was changed, the finding could suggest that the presence of other different non-electrostatic interactions, such as hydrophobic interaction, π-π bonding, hydrogen bonding, Van der Waals forces, etc., can be excluded. As for Kp, according to its pK_a value of around 4.7, [69,70] in the explored range of pH, the molecule was neutral (pH 3 < pK_a) or negatively charged (pH 6 and 12 > pK_a), and once again electrostatic repulsion occurred. Moreover, the lack of protonable amino groups in this compound confirmed, once again, the involvement of a proton-exchange mechanism of adsorption when the proposed adsorbent was in use. According to the previous findings, a possible adsorption mechanism could be hypothesized (Scheme 1).

So, the choice to pre-treated BP with NaOH and HCl can be rationalized, and therefore, experiments were also performed to find the condition during which the saturation of the selected material occurred, and the maximum adsorption capacity was thus evaluated, corresponding to 45 mg/g. It is important to highlight that the retrieved value is significant if compared with other works involving different adsorbents, both from natural or synthetic origin, reporting maximum adsorption capacities referred to CIP, ranging from a few to some thousands of mg/g (see Table 1) [25–37,40,42–46]. Specifically, the q_{max} value was in line with values referred to other natural adsorbent, but relatively low if compared with synthetic ones. However, the value can be considered high if compared with other works involving BP and others pollutants different from CIP. [13–19]

3.2.1. *Presence of salts in CIP solutions and their effects*

To better identify the supposed mechanism's presence, CIP adsorption experiments were performed in the presence of salt. Specifically, NaCl at different concentrations was used as a model electrolyte. The % of CIP adsorption was thus evaluated, and the results are reported in **Fig. S5A**. By increasing the amount of NaCl from 0.001 M to 0.5 M, the removal of CIP was hindered and completely blocked at the highest values of ionic strength. Interestingly, a remarkable change in the pH was measured during the adopted contact time. If, in the absence of salt, the observed change of pH was around 1, on the other hand, in the presence of NaCl, this value increased (**Fig. S5B**). Interestingly, the same behavior was observed in the absence of CIP, confirming the presence of an ionic exchange mechanism involving the O-based groups on the adsorbent surface. [25,27,28,31,36,60] Na^+ cations, in large excess, if compared with the CIP amount, efficiently competed for the BP active sites, and exchanged with H^+ present on the adsorbent surface. So, the pH value of the solution was significantly reduced due to the largest

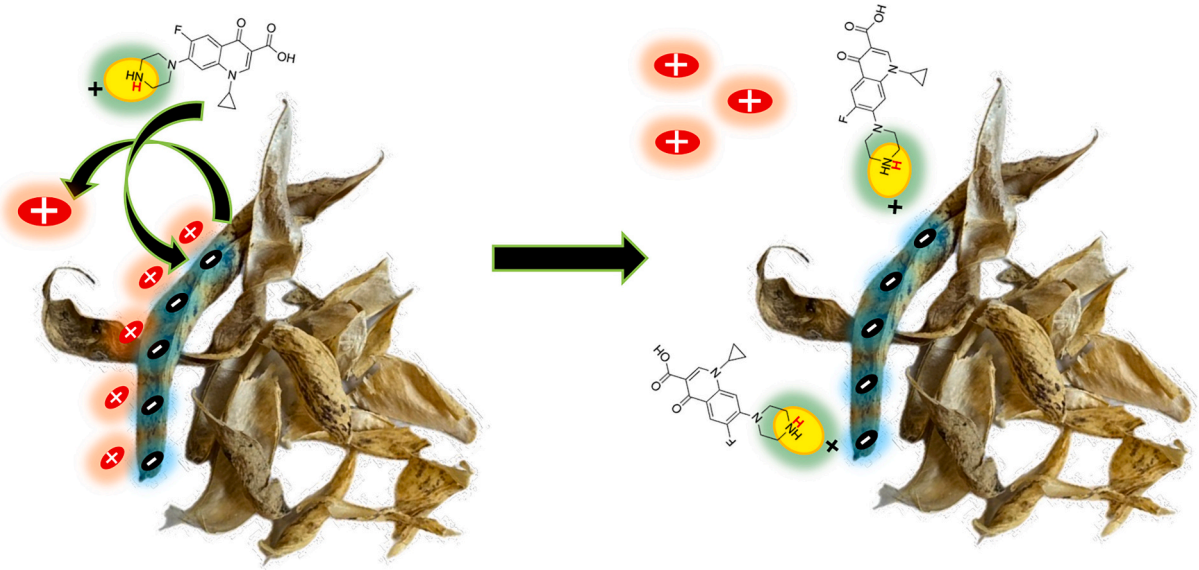

Scheme 1. Suggested ionic exchange mechanism, involved during the CIP removal by BP.

amount of Na^+. At the same time, the CIP in solution experienced a novel environment due to the pH change, and it occurred further protonated. Thus, the BP surface repelled CIP, restituting the obtained results.

3.2.2. *Effect of CIP and BP amounts on the adsorption process*

To get insight into the adsorption process, other information was obtained by studying the role of CIP and BP amounts. At first, the role of available sites on BP was assessed. For this purpose, different weights of BP were placed in a CIP solution of 10 mg/L at pH 6 and r.t. **Eqs. 1** and **2** were used to infer the % of adsorption (**Fig. 4 A**), and the adsorption capacities (**Fig. 4B**).

It was observed that when increasing the BP weights from 3 mg to 25 mg, the % of CIP removal increased, passing from 10 % to 60 % by adopting 1 h as maximum contact time. This observation suggested the importance of free active sites on the adsorbent surface that are available for ionic exchange with CIP. [25,26,36,40] By increasing the adsorbent amount, the number of O-based active sites increased, thus favoring pollutant adsorption. In agreement with this result, the related q_t values, reported in **Fig. 4B**, can better describe the process. It is worth mentioning that usually, high q_t values indicate good adsorption performances, provided that all experimental conditions are fixed and maintained constant. However, if q_t is used to compare different experimental conditions, it is important to consider that, according to **Eq. 2**, where the amount of adsorbent is the denominator of the fraction, varying the amount of adsorbent, the q_t values tend to decrease if the mass of the adsorbent increments. Accordingly, looking at **Fig. 4B**, the q_t decreased with the increase of the adsorbent amount, but it is important to highlight that, at lower BP weights, the equilibrium condition (plateau) is not reached. [25,26,36,40] In other words, the q_t values appeared to level off only at the highest amount of adsorbent, where the adsorbent's surface area was much more, therefore, richer in carbonyl functional groups, indicating that the adsorption sites were not saturated. Conversely, by reducing the amount of BP, the number of active sites decreased, and the CIP was less removed, although the q_t values were high. As reported by Chizitere Emenike et al., [4] the finding was due to the greater surface area offered by a larger amount of adsorbent. In agreement with this hypothesis, during the first time of adsorption, the CIP removal was fast due to the large presence of active sites; at the same time, the great CIP gradient of concentration enhanced the process. [25,26,36,40] At extended contact time, fewer sites were available, and the CIP concentration gradient in the solution decreased, so the CIP molecule's diffusion and adsorption collapsed. To corroborate these results, experiments were performed by changing the amount of CIP, adopting 25 mg of adsorbent as a fixed amount. Indeed, the initial concentration of the pollutant is a pivotal factor that could impact the adsorption. [25,26,36,40] **Figs. 4C** and **D** show the obtained results. The q_t values increased from the lowest to the highest CIP amount, suggesting that the CIP concentration has also a key role in the adsorption, in accordance with the previous discussion. At the same time, the collisions between the CIP molecules and BP surface should be favored at the increase of the pollutant amount, restituting high adsorption capacities. Accordingly, the changes in the % of CIP adsorption were not detected when the CIP concentration was increased. The results suggested that excess CIP molecules did not worsen the competition between the CIP for the limited number of binding sites onto the adsorbent surface. [4,25,26,36,40]

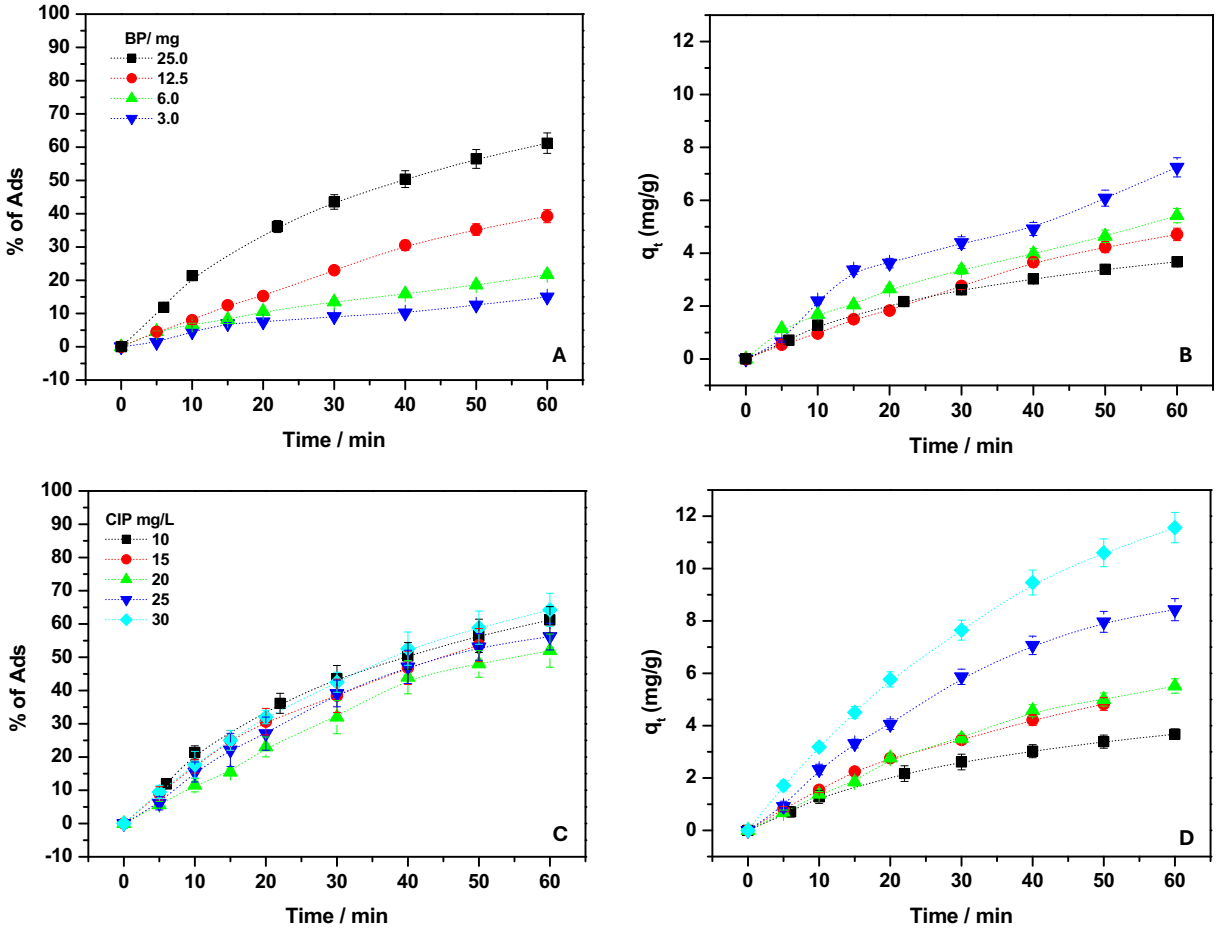

Fig. 4. % of CIP adsorption onto BP/NaOH/HCl, with the related adsorption capacities, by adopting a CIP solution of 10 mg/L, at pH 6 and r.t., and different adsorbent amounts (**A, B**) and by changing the CIP concentrations, 10–30 mg/L by fixing at 25 mg the BP amount (**C, D**).

So, from these results, it should be possible to assess that both the CIP mass transfer and its adsorption onto the BP surface had a kinetic role during the process, as better detailed in the following.

3.2.3. Kinetic analysis

To evaluate the kinetic of the process, **Eqs. 3 and 4** referred to PFO and PSO kinetic models, respectively, were applied. The attention was focused on experiments during which the effects of both CIP concentration and adsorbent amount were objects of investigation. So, the relative q_t values were rearranged according to the models, and **Figs. S6** and **S7** show the results obtained. Linear regression was thus applied to calculate the corresponding kinetic parameters (**Tables S2** and **S3**). To select the best model that well described the experimental data, the correlation coefficients R^2, and the comparison between $q_{e,exp}$ (the experimental adsorption capacities at the equilibrium, contact time 60 min) and $q_{e,calc}$ (the calculated adsorption capacities obtained by applying the kinetic equations) were taken into account. [36] From **Tables S2** and **S3**, it arose that the PFO better fitted the experimental data. Specifically, if the PFO kinetic model describes an equilibrium between the adsorbate and adsorbent, and assumes that the rate of occupation of adsorption sites is proportional to the number of unoccupied sites, as herein observed, confirming the previous discussion, on the other hand, the PSO's one assumes that the rate of adsorption sites occupation is proportional to the square of the number of unoccupied sites. At the same time, the obtained results denoted the main kinetic relevance of the CIP diffusion in the adsorption process.

In excellent agreement, the Weber-Morris model application unveiled the finding, highlighting the role of intraparticle diffusion during CIP adsorption. This model is described by **Eq. 5**, and it can be successfully applied by restituting a straight line passing from the point 0,0 when the intraparticle diffusion is the kinetic controlling step. [4,26,28,31,45] To assess this aspect, the model was used for experiments during which both the amounts of CIP and BP were changed.

By plotting the q_t values versus $t^{1/2}$, the results reported in **Fig. S8** were obtained. Cleary, a single and straight line passing through zero was used to fit experimental data, confirming the applicability of this model. So, considering the R^2 values associated with the linear regression, and reported in **Table S4**, it seemed that the internal diffusion can be considered the slower process during the CIP removal; specifically the intraparticle diffusion had a kinetic relevance during the process. As a result, the related kinetic constants were inferred (**Table S4**). In excellent agreement with the previous findings, the value of these constants increased by reducing the amount of BP and by increasing the CIP concentration. Under these conditions, the CIP gradient concentration was progressively maintained, favoring intraparticle diffusion. [4,26,28,31,45]

3.2.4. Thermodynamic analysis

To infer the thermodynamic information, the temperature role was studied during the process. So, experiments of CIP adsorption were performed in the range of temperature from 276 to 323 K with a CIP solution of 10 mg/L in the presence of 25 mg of BP. To determine the thermodynamic functions, the q_t values were calculated (**Fig. 5 A**). It was observed that the increase in temperature favored the CIP adsorption, and this evidence was especially observed at the beginning of the process when active sites were largely available. [4,25,26,36,45] So, by considering the q_t values, and the amount of the not adsorbed CIP, the K_{eq} at each temperature was inferred. **Eq. 6** was then applied to obtain the ΔG° values reported in **Table S5**.

Negative ΔG° values were found, indicating the spontaneous character of the process. **Eqs. 7** and **8** were then used to fit linearly the data obtained, reporting in the graph $\ln(K_{eq})$ vs. 1/T (**Fig. 5B**). The values of ΔH°_{298} and ΔS°_{298} were thus calculated and reported in **Table S5**. The positive values of ΔH°_{298} (+20 KJ/mol) and ΔS°_{298} (+115 J/mol × K) indicated the endothermic character of the process, and an increase of the randomness during the process, respectively. [4,25,26,36,45] It is worth mentioning that the low ΔH°_{298} value confirmed that, during the CIP removal by BP, the CIP/proton exchange mechanism regards low proton affinity sites, usually attributed to the presence of carboxylic functional groups. [60]

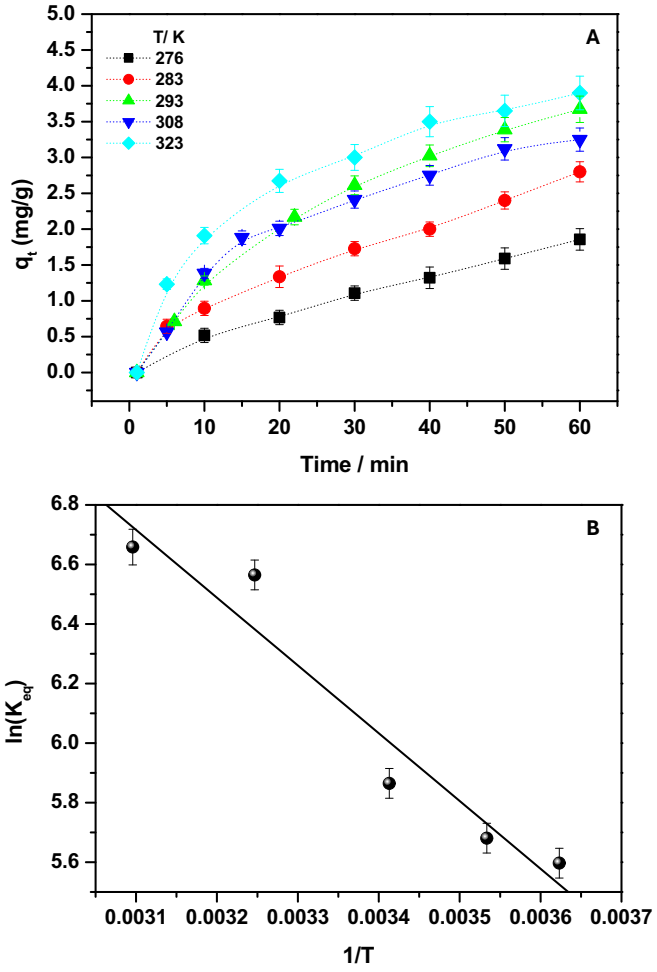

Fig. 5. q_t values of BP/NaOH/HCl calculated by changing the temperature values (from a CIP solution 10 mg/L, pH 6) (**A**); a plot of $\ln(K_{eq})$ vs 1/T to obtain ΔH° and ΔS° at 298 K (**B**).

3.2.5. Isotherms of adsorption

Langmuir, Freundlich, Temkin, and Dubinin-Radushkevitch (D-R) isotherm models (**Eqs. 9–14**) were used to search for the best model useful for describing the process. For this purpose, the R^2 values (**Table S6**) obtained from the fitting of experimental data (**Fig. S9**), were considered useful. According to the outcomes, it seemed that only the Langmuir model could not be applied (**Fig. S9A**), while the best fitting was obtained with the Freundlich isotherm (**Fig. S9B**). This behavior suggested that a single mathematical model cannot be useful to describe and predict the process. Indeed, a similar scenario was retrieved in studies involving other natural adsorbents [9–11], and the finding was justified considering the heterogeneous character of natural adsorbent having different binding sites. So, the isotherm parameters for each applied model, except for the Langmuir one, were inferred and reported in **Table S6**. On this ground, by considering the assumption of the used models, the CIP adsorption occurred on heterogeneous surfaces by forming multilayer of pollutant, the adsorbent–adsorbate interactions affected the surface coverage, and the changes in the heat of adsorption during the process occurred. It is worth mentioning that the value of the *n* parameter (see **Table S6**), inferred by applying the Freundlich equation, is representative of the adsorption strength. Particularly, values of

1/n ranging from 0 to 1, as herein observed, confirming that the physical CIP adsorption process was favored. [25,29,30,36,45] This consideration is partially confirmed by the application of the D-R model (**Fig. S9D**), from which the value of E < 8 KJ/mol (**Table S6**) indicative of physisorption can be extrapolated, although the corresponding R^2 was not satisfying.

3.3. Physicochemical features of Bean Pod after the CIP adsorption

After the CIP adsorption, ATR-FTIR, XRPD, SEM, and EDX measurements on BP were performed to infer more detailed information about the proposed approach. Interestingly, the SEM images obtained after the CIP adsorption (**Fig. S10A** and **B**) showed that, as a whole, the typical features of BP were retained, but it seemed that the small channels on the pod's surfaces and the net structures resulted in more evidenced and protruding as if covered by ribbons of solidified materials. The EDX analysis (**Fig. S10C**) was superimposable to the one obtained for the matrix before adsorption (Fig. 1P). The morphology of the CIP crystals was also investigated and occurred prismatic, as for **Fig. S10D**, and it was not identifiable on the matrix surface. According to these findings, TG and XRPD analyses (**Figs. S9-S11**) did not evidence important changes concerning the sample before its use as adsorbent, suggesting that the first CIP adsorption did not significantly alter the BP features. Other information can be obtained by the FTIR analysis performed on both sides of the BP after the CIP adsorption, and are reported in **Fig. S13**. Starting from the inner side (**Fig. S13A**), the wavenumber region 1800–1400 cm^{-1} appeared affected by CIP presence: the signals' intensity was reduced, and the intensity ratios between signals changed. Particulary, the -C=O stretching at 1745 cm^{-1} reduced its intensity, suggesting the involvement of the carboxylic moieties of BP, probably from lignin and hemicellulose, during the CIP removal. [25] The OH contribution at 3500–3000 cm^{-1} was slightly evidenced and shifted at a higher wavenumber, indicating the possible formation of H-bonds as reported in similar studies. So, the possibility that the OH moieties from alcohols present in cellulose and hemicellulose, and phenols of lignin can form H-bonds with the free electronic pairs of N, F, and O of the piperazinyl ring of the CIP can be considered. The effects on BP's outer side were insignificant (**Fig. S13B**).

3.3.1. CIP desorption and adsorbent recycling

The presence of an ionic exchange-based mechanism and the behavior observed in the presence of salt could be considered a benefit to reverse the process. So, the desorption of the adsorbed pollutant was attempted to regenerate the adsorbent. Once again, NaCl was adopted as a model electrolyte, and the effect of its concentration was evaluated. Specifically, after the CIP adsorption onto BP, the adsorbent was placed in contact with fresh water containing NaCl, and the desorption of the pollutant was monitored for 60 min. **Fig. S14A** reports the results obtained, demonstrating that the % of CIP desorption was favored by extending the contact time to 60 min and increasing the salt amount up to 0.5 M. It seemed that the solutions of NaCl 0.1 and 0.5 M are the best by obtaining the complete CIP recovery after 30 and 15 min, respectively. Furthermore, the release of the pollutant molecules occurred quickly at the beginning of the desorption process, and leveled off at extended contact time. Considering the previously hypothesized adsorption mechanism (based on CIP-proton exchange on the O-based groups at the adsorbent surface), it is possible that the cations in solutions exchanged with adsorbed CIP, and accordingly, this process induced a pronounced change of pH at greater electrolyte amounts (**Fig. S14B**). Indeed, a clear NaCl dose-dependent effect was observed, and the pH value (after CIP desorption) decreased with the increase in salt amount. As a consequence, under this experimental condition, the acidic medium favored the CIP-BP repulsion, further enhancing its desorption. At the same time, the anions should screen the positive charges of CIP and BP, slowing down the potential reverse ionic exchange. To get insight into the desorption process, the nature of salt was changed by studying the role of cations and anions. **Figs. S15** and **S16** show the obtained results, evaluating the % of CIP desorption in the presence of salts at 5, 10, and 15 min as contact time. As expected, the CIP recovering percentage increased with the contact time in all the explored conditions. However, the efficiency was different depending on the type of cation used, appearing to slightly decrease passing from K^+ to Li^+ (**Fig. S15**), suggesting that the process was sensitive to the hydrated radius increase of the cation, (K^+ = 2.32, Na^+ = 2.76, and Li^+ = 3.4 Å) and to the ion's charge density. [19] When referring to bivalent cations, despite the increase in the ionic strength, the % of Des values occurred very similar to those of monovalent-based salts. At the same time Cl^-, in large amounts, should work by screening the positive charge as previously assessed. To confirm the finding, additional experiments were thus performed. By selecting Na^+ as a cation, the nature of anions was changed, and **Fig. S16** shows the obtained results. The % of CIP recovery was compared in the presence of NaCl, NaBr, and $NaClO_4$, and the results suggested that the greater the size of the anion, the lower the CIP recovery. [25,36]

Starting from these considerations, a solution of NaCl 0.1 M was adopted for studying the ability of BP to work under continuous cycles of adsorption and desorption. Fig. 6 reports the % of the adsorbed/desorbed CIP by adopting a contact time of 60 min for each cycle. Interestingly, the % of adsorbed CIP increased from 40 % to around 75 % when the 3rd cycle was accomplished, and then remained approximately constant. On the other hand, the desorption of CIP appeared to decrease and leveled off at 20 % after the 4th cycle, as if the affinity between the pollutant and the adsorbent was increased due to an enhanced porosity of the material. The results were attributed to the partial degradation of the adsorbent mediated by the prolonged use of NaCl to desorb CIP during the consecutive adsorption/desorption cycles. [59] Indeed, the amount of retrieved adsorbent decreased from 25 to 6 mg from the beginning of the process to the last cycle.

To get insight into the process, SEM, EDX, TG, ATR-FTIR, and XRPD analyses were considered, and Figs. S10-S13 show the results obtained. In particular, the analyses were performed for the adsorbent recycled for 3 and 6 times, and compared with those referred to the adsorbent before its use. Starting from SEM analyses (**Fig. S10**), it appeared that the prolonged use of NaCl noticeably increased the number of cavities, making the material more porous as observed during the use of HCl.

Accordingly, the XRPD profile of the BP/NaCl (**Fig. S1**), referred to as BP only treated with NaCl 0.1 M, was the same as one observed for BP/NaOH/HCl, confirming the finding. The matrix was much more porous by cycling (**Figs. S10E** and **F** for 3 and 6 cycles, respectively), pointing out the fact that the adsorption and release of the CIP excavated

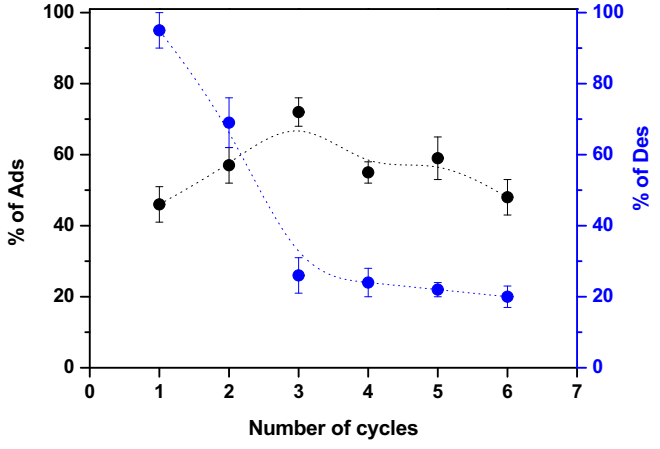

Fig. 6. % of CIP adsorption and desorption obtained after consecutive cycles of adsorption/desorption. A CIP solution 10 mg/L, pH 6, r.t. was used in the presence of 25 mg of BP/NaOH/HCl. NaCl 0.1 M was adopted for the pollutant recovery.

the substrate. This sort of chemical erosion effect exposed deeper material layers to the solution, thus increasing the affinity towards the pollutant, not favoring its release.

Accordingly, the TG measures confirmed the observations (**Fig. S12**). The typical thermogram of BP was detected (**Fig. S12A**), with the previously described weight losses; however, the DTG analysis (**Fig. S12B**) revealed the lower contribution of the signal at 200 °C, suggesting the partial decomposition of hemicellulose during the recycling. At the same time, the other two observed weight losses, mainly attributed to cellulose and lignin, were affected if compared with BP before its use; specifically, the signal previously detected at around 320 °C moved to 350 °C, and the lignin and its derived by-products contribution appeared at around 520 °C, as observed during the use of HCl, which strongly affected the material surface.

In excellent agreement with these results, as evident in **Fig. S11**, the diffraction profile of the recycled samples was superimposable with the pattern of BP/NaOH/HCl before its recycling, but the relative ratio of the two main retrieved large peaks changed; a feature better evidenced at the end of the 6th cycle. Finally, interesting results were obtained when the ATR-FTIR analysis was taken into account (**Fig. S13**). It was confirmed that that the use of NaCl altered the surface of the lignocellulosic BP, and the effect was more evident when the outer side of BP was studied.

The vibration at around 1745 cm^{-1} was weakly detected, and the signals at 2900 cm^{-1} and between 900 and 1100 cm^{-1} changed according to the formation of a new array involving lignin, cellulose, and hemicellulose, which were always retrieved in the recycled sample. Indeed, the whole adsorbent composition, as revealed by EDX, was almost unaffected by the cycles (**Figs. S10G** and **H**), with C amount a little bit lower than 50 wt% and O content around 52 wt%. In these recycled samples, Na and Si were again visible in traces.

4. Conclusions

This work discusses the use of Bean Pods, agri-food wastes, for the adsorption of emerging pollutants from water. Details about the adsorbent characterization were also presented by adopting different techniques in synergy: ATR-FTIR, TG, XRPD, BET, EDX, and SEM. The lignocellulosic nature of the material was successfully demonstrated, occurring with an irregular surface, which is potentially useful for hosting the pollutants. In particular, the effect of several treatments on the pods before their application was studied. Particularly, the washing of pods with (i) water, (ii) HCl, (iii) NaOH, and (iv), and NaOH/HCl was performed, comparing the samples. The latter treatment was selected because it favors the formation of a more porous network and enhances pollutant removal from water. For this purpose, Ciprofloxacin was adopted as a model drug, evidencing that, by increasing the temperature values, the pollutant removal from water increased. The process was spontaneous ($\Delta G^\circ < 0$), and endothermic ($\Delta H^\circ > 0$), occurring with an increase of entropy. The isotherm and the kinetic models were investigated, and it was observed that the process was defined by the Freundlich equation. The pseudo-second-order kinetic model well described the Ciprofloxacin removal by Bean Pods, with the application of the Weber-Morris model. When the effect of physical and chemical parameters on the process was studied, it was observed that the pollutant adsorption capacities increased by increasing its concentration and the adsorbent amount, suggesting the important role of free active sites on the Bean Pods surface, and Ciprofloxacin diffusion during the adsorption. The presence of electrostatic interactions between the pollutant and the adsorbent was confirmed by changing the pH values and ionic strength of the solutions containing the pollutant. Indeed, the pollutant removal occurred strongly affected, and an ionic exchange mechanism was demonstrated. On this ground, the presence of salts in solutions hindered the removal, suggesting the possibility of using them to regenerate the adsorbent, recovering the pollutant. For this purpose, NaCl 0.1 M was selected, and cycles of adsorption/desorption were performed. Work is in progress about the possibility of testing the proposed adsorbent to treat real water. Indeed, all experiments were performed by purposely contaminating water solutions, not reflecting the complexity of real wastewater (i.e., presence of competing ions, organic matter etc). In the next future, the scale up of the process will be presented by proposing the treatment of wastewater for industrial applications, focusing the attention also towards mixtures of pollutants belonging to different chemical families. Regarding this aspect, the proposed methodology should be considered environmentally friendly, lowering the disposal of agricultural wastes, favoring their reuse to solve another issue (i.e. the presence of pollutants in water). At the same time the associated costs should be favorable by considering that the adsorbent can be recycled for several time.

CRediT authorship contribution statement

Jennifer Gubitosa: Writing – review & editing, Supervision, Methodology, Investigation, Conceptualization. **Domenico Cignolo:** Software, Data curation. **Vito Rizzi:** Writing – original draft, Supervision, Funding acquisition. **Luca Pace:** Investigation. **Paola Fini:** Funding acquisition, Data curation. **Andrea Petrella:** Data curation. **Chiara Milanese:** Data curation. **Sara Paraboschi:** Data curation. **Pinalysa Cosma:** Supervision, Funding acquisition.

Declaration of competing interest

The authors declare that they have no known competing financial interests or personal relationships that could have appeared to influence the work reported in this paper.

Acknowledgements

This work was supported by the following projects: PRIN2022 “con il finanziamento del Ministero dell’Università e della Ricerca nell’ambito del Bando relativo allo scorrimento delle graduatorie finali del bando PRIN 2022” entitled: “From wastes to gold nanoparticles: CHemistRY for Sustainable And Low environmental Impact bio-circular Strategies in cancer therapy (CHRY.S.A.L.I.S.); PRIN2022-PNNR, “Finanziato dall’Unione europea – Next Generation EU” entitled “Bioderived and atomic scale engineered natural adsorbents: from water remediation to hydrogen evolution” (BECOMEH2); “MICS” (Made in Italy – Circular and Sustainable) Extended Partnership and received funding from the European Union Next-GenerationEU (PIANO NAZIONALE DI RIPRESA E RESILIENZA (PNRR)—MISSIONE 4 COMPONENTE 2, IN*VESTIMENTO* 1.3—D.D. 1551.11-10-2022, PE00000004); PRIN2022 “New cross-linked cyclodextrin-based MOFs for the removal of Emerging Contaminants”; “Fondo per la Qualità e l’Internazionalizzazione della Ricerca”, Università degli Studi di Bari “Aldo Moro”.

We kindly acknowledge Mr. Sergio Nuzzo for his technical assistance and G.P. Cassi for gifting the organic Borlotti bean pods from his private vegetable garden.

Appendix A. Supplementary data

Supplementary data to this article can be found online at https://doi.org/10.1016/j.enceco.2025.04.007.

References

[1] G.T. Tee, X.Y. Gok, W.F. Yong, Adsorption of pollutants in wastewater via biosorbents, nanoparticles and magnetic biosorbents: a review, Environ. Res. 212 (2022) 113248, https://doi.org/10.1016/j.envres.2022.113248.

[2] M. Ahmed, M.O. Mavukkandy, A. Giwa, M. Elektorowicz, E. Katsou, O. Khelifi, V. Naddeo, S.W. Hasan, Recent developments in hazardous pollutants removal from wastewater and water reuse within a circular economy, Npj Clean Water 5 (2022) 12, https://doi.org/10.1038/s41545-022-00154-5.

[3] S. Kathi, A. El Din Mahmoud, Trends in effective removal of emerging contaminants from wastewater: a comprehensive review, Desalin. Water Treat. 317 (2024) 100258, https://doi.org/10.1016/j.dwt.2024.100258.
[4] E.C. Emenike, H.K. Okoro, A.G. Adeniyi, K.O. Iwuozor, C. Zvinowanda, J.C. Ngila, Applications of bean pod and husk for remediation of water contamination: a review, Bioresour. Technol. Reports 25 (2024) 101754, https://doi.org/10.1016/j.biteb.2023.101754.
[5] B.S. Rathi, P.S. Kumar, Application of adsorption process for effective removal of emerging contaminants from water and wastewater, Environ. Pollut. 280 (2021) 116995, https://doi.org/10.1016/j.envpol.2021.116995.
[6] A.M. Badran, U. Utra, N.S. Yussof, M.J.K. Bashir, Advancements in adsorption techniques for sustainable water purification: a focus on Lead removal, Separations 10 (2023), https://doi.org/10.3390/separations10110565.
[7] A. Benettayeb, S. Ahamadi, S. Ghosh, M. Malbenia John, C.R. Mitchel, B. Haddou, Chapter 4 - Natural adsorbents for the removal of emerging pollutants and its adsorption mechanisms, in: M. Hadi Dehghani, R.R. Karri, I.B.T.-S.R.T. for E.P (Eds.), A.E. Tyagi, Elsevier, 2024, pp. 63–78, https://doi.org/10.1016/B978-0-443-18618-9.00013-9.
[8] J. Li, Y. Liu, J. Wang, Y. Liu, M. Zhang, L. Zhao, S. Gu, R. Lin, L. Chen, Research progress on the application of natural adsorbents in the treatment of livestock wastewater, Desalin. Water Treat. 317 (2024) 100018, https://doi.org/10.1016/j.dwt.2024.100018.
[9] V. Rizzi, J. Gubitosa, P. Fini, A. Petrella, R. Romita, A. Agostiano, P. Cosma, A "classic" material for capture and detoxification of emergent contaminants for water purification: the case of tetracycline, Environ. Technol. Innov. 19 (2020) 100812, https://doi.org/10.1016/j.eti.2020.100812.
[10] V. Rizzi, F. Romanazzi, J. Gubitosa, P. Fini, R. Romita, A. Agostiano, A. Petrella, P. Cosma, Chitosan film as eco-friendly and recyclable bio-adsorbent to remove/recover diclofenac, Ketoprofen, and their Mixture from Wastewater, Biomolecules 9 (2019) 571, https://doi.org/10.3390/biom9100571.
[11] V. Rizzi, D. Lacalamita, J. Gubitosa, P. Fini, A. Petrella, R. Romita, A. Agostiano, J. A.J.A. Gabaldón, M.I.M.I. Fortea Gorbe, T. Gómez-Morte, P. Cosma, Removal of tetracycline from polluted water by chitosan-olive pomace adsorbing films, Sci. Total Environ. 693 (2019) 133620, https://doi.org/10.1016/j.scitotenv.2019.133620.
[12] P. Bianchini, F. Merlo, V. Quarta, L. Ferrari, C. Milanese, A. Profumo, A. Speltini, Improving sample preparation by biochar-coated sampling tubes: proof-of-concept extraction of sex hormones from real waters, Adv. Sample Prep. 12 (2024) 100129, https://doi.org/10.1016/j.sampre.2024.100129.
[13] I.C. De Sá, P.M. Oliveira Silva, E. Nossol, P.H.S. Borges, F.G. Lepri, F.S. Semaan, R. M. Dornellas, W.F. Pacheco, Modified dry bean pod waste (Phaseolus vulgaris) as a biosorbent for fluorescein removal from aqueous media: batch and fixed bed studies, J. Hazard. Mater. 424 (2022) 127723, https://doi.org/10.1016/j.jhazmat.2021.127723.
[14] L. Akinola, A. Umar, Adsorption of crystal violet onto adsorbents derived from agricultural wastes: kinetic and equilibrium studies, J. Appl. Sci. Environ. Manag. 19 (2015) 279–288, https://doi.org/10.4314/jasem.v19i2.15.
[15] T. Budinova, D. Savova, B. Tsyntsarski, C.O. Ania, B. Cabal, J.B. Parra, N. Petrov, Biomass waste-derived activated carbon for the removal of arsenic and manganese ions from aqueous solutions, Appl. Surf. Sci. 255 (2009) 4650–4657, https://doi.org/10.1016/j.apsusc.2008.12.013.
[16] B. Cabal, T. Budinova, C.O. Ania, B. Tsyntsarski, J.B. Parra, B. Petrova, Adsorption of naphthalene from aqueous solution on activated carbons obtained from bean pods, J. Hazard. Mater. 161 (2009) 1150–1156, https://doi.org/10.1016/j.jhazmat.2008.04.108.
[17] G. Mosoarca, S. Popa, C. Vancea, S. Boran, Optimization, equilibrium and kinetic modeling of methylene blue removal from aqueous solutions using dry bean pods husks powder, Materials (Basel). 14 (2021), https://doi.org/10.3390/ma14195673.
[18] G. Mosoarca, C. Vancea, S. Popa, S. Boran, M.E. Radulescu-Grad, Crystal violet removal from aqueous solutions using dry bean pods husks powder – optimization and desorption studies, Ovidius Univ. Ann. Chem. 33 (2022) 129–134, https://doi.org/10.2478/auoc-2022-0019.
[19] G.F. Nindjio, R.F. Tagne, S.L. Jiokeng, C.G. Fotsop, A. Bopda, G. Doungmo, R. C. Temgoua, I. Doench, E.T. Njoyim, A.K. Tamo, A. Osorio-Madrazo, I.K. Tonle, Lignocellulosic-based materials from bean and pistachio pod wastes for dye-contaminated water treatment: optimization and modeling of indigo carmine sorption, Polymers (Basel). 14 (2022), https://doi.org/10.3390/polym14183776.
[20] S. Sert Çok, F. Koç, A. Len, L. Almásy, Z. Dudás, Silica aerogels modified with vinyl, epoxide, methacrylate moieties for the removal of ciprofloxacin by adsorption from water, Sep. Purif. Technol. 354 (2025) 129112, https://doi.org/10.1016/j.seppur.2024.129112.
[21] P. Barathe, K. Kaur, S. Reddy, V. Shriram, V. Kumar, Antibiotic pollution and associated antimicrobial resistance in the environment, J. Hazard. Mater. Lett. 5 (2024) 100105, https://doi.org/10.1016/j.hazl.2024.100105.
[22] A. Singh, S.G. Pratap, A. Raj, Occurrence and dissemination of antibiotics and antibiotic resistance in aquatic environment and its ecological implications: a review, Environ. Sci. Pollut. Res. 31 (2024) 47505–47529, https://doi.org/10.1007/s11356-024-34355-x.
[23] P. Mishra, G. Tripathi, V. Mishra, T. Ilyas, S. Irum, S. Firdaus, A. Ahmad, N. Farooqui, S. Yadav, S. Rustagi, R. Shreaz, A.N. Yadav Negi, Antibiotic contamination in wastewater treatment plant effluents: current research and future perspectives, Environ. Nanotechnology, Monit. Manag. 23 (2025) 101047, https://doi.org/10.1016/j.enmm.2025.101047.
[24] P. Chen, Z. Zhu, Z. Liu, F. Liang, X. Zhu, Z. Bin, F. Huang, N. Wang, Y. Zhu, Efficient removal of ciprofloxacin from water by BiOX/GaMOF S-scheme heterojunction: a synergistic effect of adsorption and photocatalysis, Chem. Eng. J. 506 (2025) 159689, https://doi.org/10.1016/j.cej.2025.159689.
[25] J. Gubitosa, V. Rizzi, D. Cignolo, P. Fini, F. Fanelli, P. Cosma, From agricultural wastes to a resource: kiwi peels, as long-lasting, recyclable adsorbent, to remove emerging pollutants from water. The case of ciprofloxacin removal, Sustain. Chem. Pharm. 29 (2022) 100749, https://doi.org/10.1016/j.scp.2022.100749.
[26] M.E. Peñafiel, J.M. Matesanz, E. Vanegas, D. Bermejo, R. Mosteo, M.P. Ormad, Comparative adsorption of ciprofloxacin on sugarcane bagasse from Ecuador and on commercial powdered activated carbon, Sci. Total Environ. 750 (2021) 141498, https://doi.org/10.1016/j.scitotenv.2020.141498.
[27] B. Gao, Q. Chang, H. Yang, Selective adsorption of ofloxacin and ciprofloxacin from a binary system using lignin-based adsorbents: quantitative analysis, adsorption mechanisms, and structure-activity relationship, Sci. Total Environ. 765 (2021) 144427, https://doi.org/10.1016/j.scitotenv.2020.144427.
[28] H. Ji, T. Wang, T. Huang, B. Lai, W. Liu, Adsorptive removal of ciprofloxacin with different dissociated species onto titanate nanotubes, J. Clean. Prod. 278 (2021) 123924, https://doi.org/10.1016/j.jclepro.2020.123924.
[29] J. Li, L. Pan, G. Yu, C. Li, S. Xie, Y. Wang, Synthesis of an easily recyclable and safe adsorbent from sludge pyrochar for ciprofloxacin adsorption, Environ. Res. 192 (2021) 110258, https://doi.org/10.1016/j.envres.2020.110258.
[30] Y. Ma, M. Li, P. Li, L. Yang, L. Wu, F. Gao, X. Qi, Z. Zhang, Hydrothermal synthesis of magnetic sludge biochar for tetracycline and ciprofloxacin adsorptive removal, Bioresour. Technol. 319 (2021) 124199, https://doi.org/10.1016/j.biortech.2020.124199.
[31] Y. Fu, Z. Yang, Y. Xia, Y. Xing, X. Gui, Adsorption of ciprofloxacin pollutants in aqueous solution using modified waste grapefruit peel, energy sources, Part A Recover. Util. Environ. Eff. 43 (2021) 225–234, https://doi.org/10.1080/15567036.2019.1624877.
[32] L. Wang, C. Yang, A. Lu, S. Liu, Y. Pei, X. Luo, An easy and unique design strategy for insoluble humic acid/cellulose nanocomposite beads with highly enhanced adsorption performance of low concentration ciprofloxacin in water, Bioresour. Technol. 302 (2020) 122812, https://doi.org/10.1016/j.biortech.2020.122812.
[33] D. Lu, S. Xu, W. Qiu, Y. Sun, X. Liu, J. Yang, J. Ma, Adsorption and desorption behaviors of antibiotic ciprofloxacin on functionalized spherical MCM-41 for water treatment, J. Clean. Prod. 264 (2020) 121644, https://doi.org/10.1016/j.jclepro.2020.121644.
[34] C. Zheng, H. Zheng, C. Hu, Y. Wang, Y. Wang, C. Zhao, W. Ding, Q. Sun, Structural design of magnetic biosorbents for the removal of ciprofloxacin from water, Bioresour. Technol. 296 (2020) 122288, https://doi.org/10.1016/j.biortech.2019.122288.
[35] H. Zhang, S.K. Khanal, Y. Jia, S. Song, H. Lu, Fundamental insights into ciprofloxacin adsorption by sulfate-reducing bacteria sludge: mechanisms and thermodynamics, Chem. Eng. J. 378 (2019) 122103, https://doi.org/10.1016/j.cej.2019.122103.
[36] V. Rizzi, J. Gubitosa, R. Signorile, P. Fini, C. Cecone, A. Matencio, F. Trotta, P. Cosma, Cyclodextrin nanosponges as adsorbent material to remove hazardous pollutants from water: the case of ciprofloxacin, Chem. Eng. J. 411 (2021) 128514, https://doi.org/10.1016/j.cej.2021.128514.
[37] M.K. Mohammadi Nodeh, S. Soltani, S. Shahabuddin, H. Rashidi Nodeh, H. Sereshti, Equilibrium, kinetic and thermodynamic study of magnetic polyaniline/graphene oxide based nanocomposites for ciprofloxacin removal from water, J. Inorg. Organomet. Polym. Mater. 28 (2018) 1226–1234, https://doi.org/10.1007/s10904-018-0782-2.
[38] S. Li, X. Zhang, Y. Huang, Zeolitic imidazolate framework-8 derived nanoporous carbon as an effective and recyclable adsorbent for removal of ciprofloxacin antibiotics from water, J. Hazard. Mater. 321 (2017) 711–719, https://doi.org/10.1016/j.jhazmat.2016.09.065.
[39] F. Zhao, E. Repo, D. Yin, L. Chen, S. Kalliola, J. Tang, E. Iakovleva, K.C. Tam, M. Sillanpää, One-pot synthesis of trifunctional chitosan-EDTA-β-cyclodextrin polymer for simultaneous removal of metals and organic micropollutants, Sci. Rep. 7 (2017) 15811, https://doi.org/10.1038/s41598-017-16222-7.
[40] A. Azizi, Green synthesis of iron oxide/cellulose magnetic recyclable nanocomposite and its evaluation in ciprofloxacin removal from aqueous solutions, J. Iran. Chem. Soc. 18 (2021) 331–341, https://doi.org/10.1007/s13738-020-02028-4.
[41] M.Z. Afzal, X.-F. Sun, J. Liu, C. Song, S.-G. Wang, A. Javed, Enhancement of ciprofloxacin sorption on chitosan/biochar hydrogel beads, Sci. Total Environ. 639 (2018) 560–569, https://doi.org/10.1016/j.scitotenv.2018.05.129.
[42] A. Ashiq, B. Sarkar, N. Adassooriya, J. Walpita, A.U. Rajapaksha, Y.S. Ok, M. Vithanage, Sorption process of municipal solid waste biochar-montmorillonite composite for ciprofloxacin removal in aqueous media, Chemosphere 236 (2019) 124384, https://doi.org/10.1016/j.chemosphere.2019.124384.
[43] N.A. Khan, T. Najam, S.S.A. Shah, E. Hussain, H. Ali, S. Hussain, A. Shaheen, K. Ahmad, M. Ashfaq, Development of Mn-PBA on GO sheets for adsorptive removal of ciprofloxacin from water: kinetics, isothermal, thermodynamic and mechanistic studies, Mater. Chem. Phys. 245 (2020) 122737, https://doi.org/10.1016/j.matchemphys.122737.
[44] F. Yu, D. Chen, J. Ma, Adsorptive removal of ciprofloxacin by ethylene diaminetetraacetic acid/β-cyclodextrin composite from aqueous solution, New J. Chem. 42 (2018) 2216–2223, https://doi.org/10.1039/C7NJ03770H.
[45] B. Hao, F. Wang, H. Huang, Y. Wu, S. Jia, Y. Liao, H. Mao, Tannin foam immobilized with ferric ions for efficient removal of ciprofloxacin at low concentrations, J. Hazard. Mater. 414 (2021) 125567, https://doi.org/10.1016/j.jhazmat.2021.125567.
[46] S.I. Eze, K.G. Akpomie, O.M. Ezekoye, C.N. Chukwujindu, F.K. Ojo, J.U. Ani, O. T. Ujam, Antibiotic adsorption by acid enhanced Dialium guineense seed waste,

Arab. J. Sci. Eng. 46 (2021) 309–324, https://doi.org/10.1007/s13369-020-04771-5.
[47] B. Mu, H. Wang, X. Hao, Q. Wang, Morphology, mechanical properties and dimensional stability of biomass particles/high density polyethylene composites: effect of species and composition, Polymers (Basel). 10 (2018), https://doi.org/10.3390/polym10030308.
[48] J. Perel, An X-ray study of regain-dependent deformations in cotton crystallites, J. Text. Inst. 81 (1990) 241–244, https://doi.org/10.1080/00405009008658707.
[49] A. El Oudiani, Y. Chaabouni, S. Msahli, F. Sakli, Crystal transition from cellulose I to cellulose II in NaOH treated Agave Americana L. fibre, Carbohydr. Polym. 86 (2011) 1221–1229, https://doi.org/10.1016/j.carbpol.2011.06.037.
[50] R.A.C. Gomide, A.C.S. de Oliveira, D.A.C. Rodrigues, C.R. de Oliveira, O.B.G. de Assis, M.V. Dias, S.V. Borges, Development and characterization of lignin microparticles for physical and antioxidant enhancement of biodegradable polymers, J. Polym. Environ. 28 (2020) 1326–1334, https://doi.org/10.1007/s10924-020-01685-z.
[51] J. Wang, J. Zhao, X. He, Y. Qiao, L. Li, S.-L. Chou, Hard carbon derived from hazelnut shell with facile HCl treatment as high-initial-coulombic-efficiency anode for sodium ion batteries, Sustain. Mater. Technol. 33 (2022) e00446, https://doi.org/10.1016/j.susmat.2022.e00446.
[52] M.V. Kok, E. Ozgur, Characterization of lignocellulose biomass and model compounds by thermogravimetry, energy sources, Part A Recover. Util. Environ. Eff. 39 (2017) 134–139, https://doi.org/10.1080/15567036.2016.1214643.
[53] G.S.C. Raulino, L.S. da Silva, C.B. Vidal, E. de Sousa Almeida, D. de Quadros Melo, R.F. Nascimento, Role of surface chemistry and morphology in the reactive adsorption of metal ions on acid modified dry bean pods (Phaseolus vulgaris L.) organic polymers, J. Appl. Polym. Sci. 135 (2018) 45879, https://doi.org/10.1002/app.45879.
[54] J. Escalante, W.-H. Chen, M. Tabatabaei, A.T. Hoang, E.E. Kwon, K.-Y. Andrew Lin, A. Saravanakumar, Pyrolysis of lignocellulosic, algal, plastic, and other biomass wastes for biofuel production and circular bioeconomy: a review of thermogravimetric analysis (TGA) approach, renew, Sustain. Energy Rev. 169 (2022) 112914, https://doi.org/10.1016/j.rser.2022.112914.
[55] F.A. Aguilar-Aguilar, V.Y. Mena-Cervantes, C. Romero-Hernández, F.S. Mederos-Nieto, A. Ramírez- Estada, R. Hernández-Altamirano, Thermal, structural, and compositional evaluation of coyol shell pretreatments for enhanced lignocellulosic biomass utilization, Biomass Bioenergy 193 (2025) 107518, https://doi.org/10.1016/j.biombioe.2024.107518.
[56] S.G. Kostryukov, H.B. Matyakubov, Y.Y. Masterova, A.S. Kozlov, M. K. Pryanichnikova, A.A. Pynenkov, N.A. Khluchina, Determination of lignin, cellulose, and hemicellulose in plant materials by FTIR spectroscopy, J. Anal. Chem. 78 (2023) 718–727, https://doi.org/10.1134/S1061934823040093.
[57] Z. Jiang, J. Yi, J. Li, T. He, C. Hu, Promoting effect of sodium chloride on the Solubilization and Depolymerization of cellulose from raw biomass materials in water, ChemSusChem 8 (2015) 1901–1907, https://doi.org/10.1002/cssc.201500158.
[58] Y. Bouramdane, S. Fellak, F. El Mansouri, A. Boukir, Impact of natural degradation on the aged lignocellulose fibers of Moroccan cedar softwood: structural elucidation by infrared spectroscopy (ATR-FTIR) and X-ray diffraction (XRD), Fermentation 8 (2022), https://doi.org/10.3390/fermentation8120698.
[59] V. Volli, A.R.K. Gollakota, C.-M. Shu, Comparative studies on thermochemical behavior and kinetics of lignocellulosic biomass residues using TG-FTIR and Py-GC/MS, Sci. Total Environ. 792 (2021) 148392, https://doi.org/10.1016/j.scitotenv.2021.148392.
[60] X.-T. Zhao, T. Zeng, Z.J. Hu, H.-W. Gao, C.Y. Zou, Modeling and mechanism of the adsorption of proton onto natural bamboo sawdust, Carbohydr. Polym. 87 (2012) 1199–1205, https://doi.org/10.1016/j.carbpol.2011.08.098.
[61] Y. Chen, F. Wang, L. Duan, H. Yang, J. Gao, Tetracycline adsorption onto rice husk ash, an agricultural waste: its kinetic and thermodynamic studies, J. Mol. Liq. 222 (2016) 487–494, https://doi.org/10.1016/j.molliq.2016.07.090.
[62] J. Gubitosa, V. Rizzi, P. Fini, S. Nuzzo, P. Cosma, Regenerable kiwi peels as an adsorbent to remove and reuse the emerging pollutant propranolol from water, Process 10 (2022), https://doi.org/10.3390/pr10071417.
[63] T. Wang, Z. Zhang, H. Zhang, X. Zhong, Y. Liu, S. Liao, X. Yue, G. Zhou, Sorption of carbendazim on activated carbons derived from rape straw and its mechanism, RSC Adv. 9 (2019) 41745–41754, https://doi.org/10.1039/C9RA06495H.
[64] J.A. Arancibia, G.M. Escandar, Complexation study of diclofenac with β-cyclodextrin and spectrofluorimetric determination, Analyst 124 (1999) 1833–1838, https://doi.org/10.1039/A906719A.
[65] S. Salvestrini, A. Fenti, S. Chianese, P. Iovino, D. Musmarra, Diclofenac sorption from synthetic water: kinetic and thermodynamic analysis, J. Environ. Chem. Eng. 8 (2020) 104105, https://doi.org/10.1016/j.jece.2020.104105.
[66] C.D. Herzfeldt, R. Kümmel, Dissociation constants, solubilities and dissolution rates of some selected nonsteroidal antiinflammatories, Drug Dev. Ind. Pharm. 9 (1983) 767–793, https://doi.org/10.3109/03639048309039887.
[67] B.N. Bhadra, P.W. Seo, S.H. Jhung, Adsorption of diclofenac sodium from water using oxidized activated carbon, Chem. Eng. J. 301 (2016) 27–34, https://doi.org/10.1016/j.cej.2016.04.143.
[68] M.A. Décima, S. Marzeddu, M. Barchiesi, C. Di Marcantonio, A. Chiavola, M. R. Boni, A review on the removal of carbamazepine from aqueous solution by using activated carbon and biochar, Sustainability 13 (2021), https://doi.org/10.3390/su132111760.
[69] A.F.M. Streit, G.C. Collazzo, S.P. Druzian, R.S. Verdi, E.L. Foletto, L.F.S. Oliveira, G. L. Dotto, Adsorption of ibuprofen, ketoprofen, and paracetamol onto activated carbon prepared from effluent treatment plant sludge of the beverage industry, Chemosphere 262 (2021) 128322, https://doi.org/10.1016/j.chemosphere.2020.128322.
[70] A.C. Fröhlich, G.S. dos Reis, F.A. Pavan, É.C. Lima, E.L. Foletto, G.L. Dotto, Improvement of activated carbon characteristics by sonication and its application for pharmaceutical contaminant adsorption, Environ. Sci. Pollut. Res. 25 (2018) 24713–24725, https://doi.org/10.1007/s11356-018-2525-x.